Lawrence Berkeley National Laboratory

Title

Fluorosulfates of graphite and boron nitride and other high oxidation state studies

Permalink

https://escholarship.org/uc/item/3fx790zv

Author

Biagoni, Richard N.

Publication Date

1980-10-01

Lawrence Berkeley Laboratory
UNIVERSITY OF CALIFORNIA

Materials & Molecular Research Division

FLUOROSULFATES OF GRAPHITE AND BORON NITRIDE AND
OTHER HIGH OXIDATION STATE STUDIES

Richard N. Biagioni
(Ph.D. thesis)

October 1980

DISCLAIMER

LBL-11760

FLUOROSULFATES OF GRAPHITE AND BORON NITRIDE AND OTHER HIGH OXIDATION STATE STUDIES

Richard N. Biagioni

Materials and Molecular Research Division
Lawrence Berkeley Laboratory and Department of Chemistry
University of California, Berkeley, California 94720

CONTENTS

Fluorosulfates of Graphite and Boron Nitride and
Other High Oxidation State Studies

Richard N. Biagioni

Materials and Molecular Research Division
Lawrence Berkeley Laboratory and Department of Chemistry
University of California, Berkeley, California 94720

ABSTRACT

The previously known adduct $XeF_2 \cdot AsF_5$ was re-examined. Based on Raman and structural information, the compound was assessed to be intermediate between the salt formulation $(FXe)^+ AsF_6^-$ and the fluorine bridged molecular adduct.

A series of graphite fluorosulfates were prepared, using as the oxidizing agent $S_2O_6F_2$, and the effects of incorporating varying amounts of fluorosulfonic acid were studied. Physical data indicated that the $S_2O_6F_2$ was incorporated as SO_3F^-, and the HSO_3F was bound tightly, probably due to hydrogen bonding. The c-spacings of HSO_3F containing materials were larger than those of acid free materials, and the influences of charging, guest size and guest orientation were examined.

X-ray diffractometer studies of graphite "slabs" intercalated with SO_3F/HSO_3F and IrF_6 indicated structures consistent with the characterization of these materials as containing tetrahedral SO_3F and octahedral IrF_6.

Boron nitride reacted with $S_2O_6F_2$ to yield a deep blue, conducting intercalation compound. This material was in many respects similar to its graphite analog, but chemically more labile.

I. INTRODUCTION

This thesis is composed of four major chapters. Chapter II describes the characterization of $XeF_2 \cdot AsF_5$. Chapters III and IV comprise the bulk of the work presented here. Chapter III deals with the synthesis and characterization of the graphite fluorosulfate system, and Chapter IV with some structural studies of graphite fluorosulfate and graphite hexafluoroiridate. The last chapter describes the synthesis and characterization of boron nitride fluorosulfate.

A. Working apparatus and material handling

1. <u>Vacuum lines</u>. Most of the compounds handled in this work were quite air sensitive and corrosive, requiring the use of a metal vacuum line. Initially, some high pressure fluorine work was anticipated, so the original vacuum line was very similar to other systems being used in the laboratory at the time, using high pressure valves and narrow bore heavy wall tubing.[1] This type of system, with some modification, was used for the first four years of this work.

However, the narrow bore tubing, which was subject to serious buildups of particulate matter, particularly when used to handle fluorosulfates, proved to be a serious drawback. This problem, along with the realization that high pressure capability was seldom needed, leads to the construction of a new line.

The new line shown diagramatically in Figure 1-1, was a hybrid of 316 stainless steel Hoke (Cresskill, N.J.) diaphragm valves connected by wide bore stainless steel tubing for general work, and a smaller portion composed of Autoclave Engineering (Erie, Penn.) Series 30 mo-

nel valves (rated to 30,000 psi) and narrow bore tubing and appropriate connectors, for fluorine and high pressure service. Working pressures were monitored by a 0–1500 torr Helicoid (Bridgeport, Conn.) gauge and pressures below 1 torr by a Hastings thermocouple gauge. The system was fitted with a good quality mechanical pump for general work, and a smaller pump connected through a soda lime tower to dispose of waste fluorine.

This line was used primarily as a vacuum manifold. Smaller temporary systems, constructed of either monel or stainless steel Whitey (Cleveland, Ohio) IKS4 valves and appropriate connectors, were attached to this for synthetic work.

2. Reaction vessels. A wide variety of reaction vessels and storage containers was used. Whitey IKS4 valves (monel, stainless steel, or brass, depending on application and availability) were used for general purposes. Kel-F valves (fabricated by the mechanical shop) were employed when metal and glass components were not suitable. Reaction vessels were made of fused silica glass (quartz), borosilicate glass (Pyrex), Teflon FEP, or Kel-F, and connected to the valves via Swagelok, Gyrolok, or occasionally home-made fittings. Quartz and Pyrex, usually available in metric sizes, could be employed with SAE fittings which had been bored out, and a vacuum tight seal easily attained by using Teflon TFE ferrules. For applications requiring pressures greater than two atmospheres, monel cans and bulbs of various sizes were used.

In some instances, particularly in the use of fluorosulfonic acid, the use of metal components was undesirable. For these applications, glass systems employing breakseals or glass-Teflon valves were employed. Kontes valves, once their Viton o-rings had been replaced, were found to give satisfactory service. The valve stem o-rings were replaced with Teflon coated Buna-N o-rings (Porter Seal Co., Oakland), and the valve tip o-rings with solid Teflon o-rings. Lightly lubricating the valve stem o-rings with chlorofluorocarbon wax (Series 40, Halocarbon Corp., Hackensack, N.J.) improved valve service.

3. Glove boxes. Reactive solids were handled in a Vacuum Atmospheres Corp. (North Hollywood, CA.) nitrogen atmosphere Dri Lab, equipped with a circulating purifier to remove oxygen and water. The inlet port to the purifier was fitted with a sodium hydroxide trap to prevent corrosive materials from damaging the purifier. Work requiring the pouring of moderately volatile corrosive liquids was carried out in either a glovebag or a small glovebox purged with nitrogen.

4. Leak detection. Assembled apparatus was leak tested using a CEC24-120B helium mass spectrometer leak detector (Consolidated Electrodynamics Corp. Monrovia, CA.). Glass systems could also be tested with a tesla coil.

B. Routine characterization of materials

1. Infrared. For the first three years of this work, a Perkin Elmer model 337 Grating Spectrophotometer was used. A Perkin Elmer 597 was used for the remainder of the work. Gas phase spectra were obtained

using either an 8 cm pathlength monel cell, or a 7 cm pathlength Kel- F
cell, each fitted with silver chloride windows (Harshaw Chemical Co,
Cleveland, Ohio). The cells were passivated by gentle fluorination
with fluorine after each disassembly.

2. Raman spectroscopy. Initially, Raman spectra were obtained using
a Cary 83 spectrometer, using 488 nm light from an argon laser.
Later, a J-Y Ramanor HG.2S spectrometer with a double holographic
grating monochrometer was employed. This could be used with either
an argon laser (514 nm or 488 nm) or a krypton laser (647 nm).

Generally, solid samples were enclosed in capillaries in the Dri-
Lab, plugged with Kel-F grease, and then sealed with a microtorch out-
side the drybox. Liquid samples were contained in vessels of various
shapes and sizes, made of quartz, Pyrex, or Teflon FEP.

To allow low temperature studies, a cooling apparatus was con-
structed shown diagramatically in Figure 1-2. The sample was cooled
by a stream of cold nitrogen, shrouded by a stream of room tempera-
ture dry nitrogen to prevent moisture from condensing on the sample.
Two exhausts connected to house vacuum kept the nitrogen flow stream-
lined. Flowrates for each jet could be regulated independently.
Temperatures were measured using a copper-constantan thermocouple.
Samples were contained in tubes less than 1/4 inch diameter. Capil-
laries were attached to the end of a rod. Temperatures as low as
-140°C were attainable.

3. X-ray powder photography. X-ray powder diffraction patterns were
obtained using a General Electric Co. Precision camera (circumference

45 cm), using Ni filtered Cu Kα radiation. Powdered samples were loaded into thin walled quartz capillaries, as for powdered Raman samples. Samples would be cooled with a stream of cold nitrogen shrouded by room temperature nitrogen, using a Dewar jet similar to that used for the Raman low temperature device. An automatic filling apparatus connected to a 50 liter reservoir of liquid nitrogen allowed low temperature maintainance for approximately twelve hours per fill. Films were measured using a Norelco measuring device.

4. X-ray precession photography. X-ray precession photographs were obtained on either a Nonius or Supper camera, using Zr filtered Mo Kα radiation, and Polaroid Type 57 film. Samples were contained in sealed quartz capillaries. Photographs were measured using a Supper measuring device.

5. Special techniques and equipment. To be described in the appropriate chapters.

REFERENCE

1. See Ph.D. thesis of K. Leary, University of California, Berkeley, (1975).

Figure 1-1. Vacuum line.

Soda lime tower

Helicoid gauge (M)

Thermocouple gauge

To F$_2$ cylinder

To small mechanical pump

To mechanical pump

Pyrex cold traps

Whitey valve

Hoke valve

Autoclave engineering valve

(M)   Monel
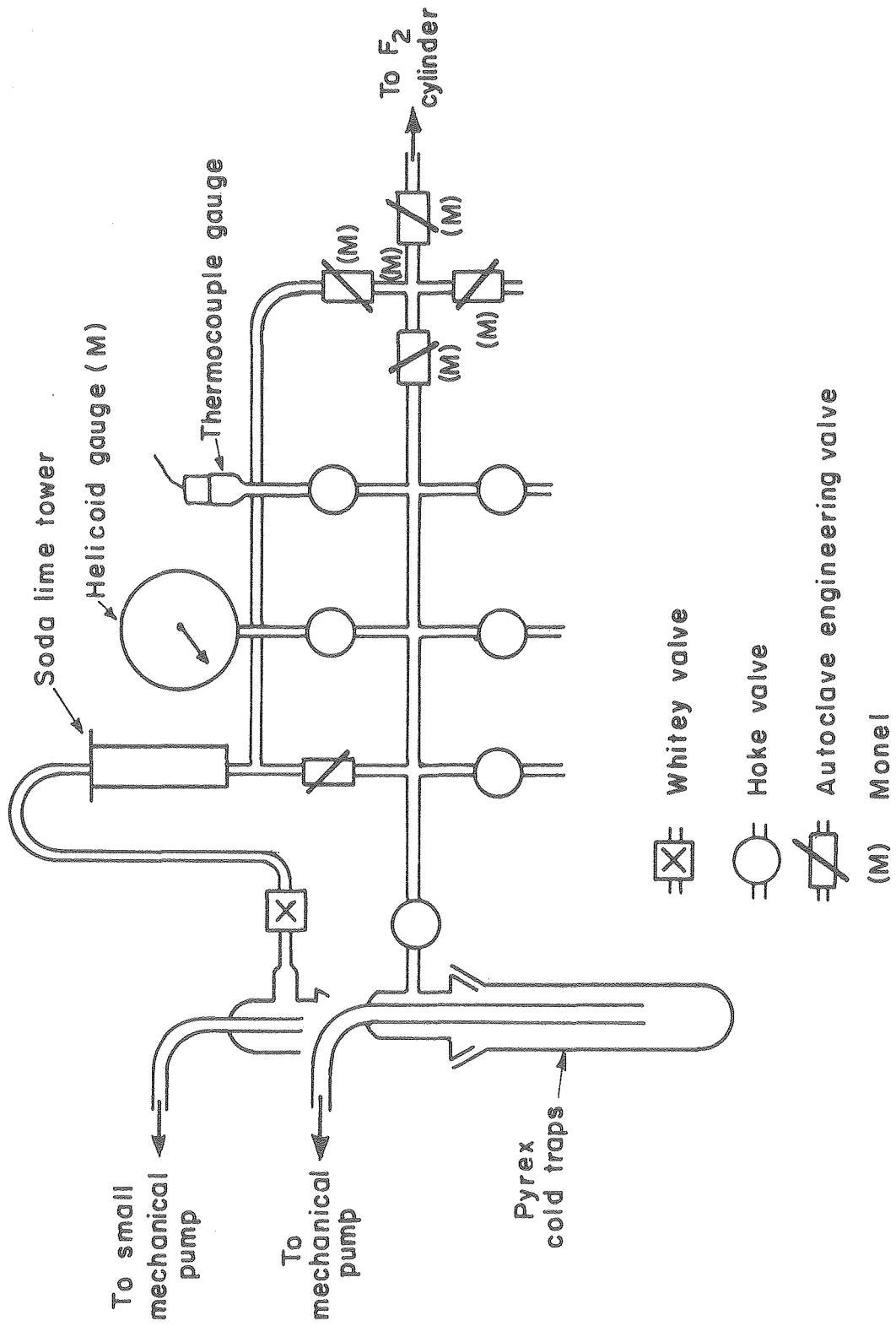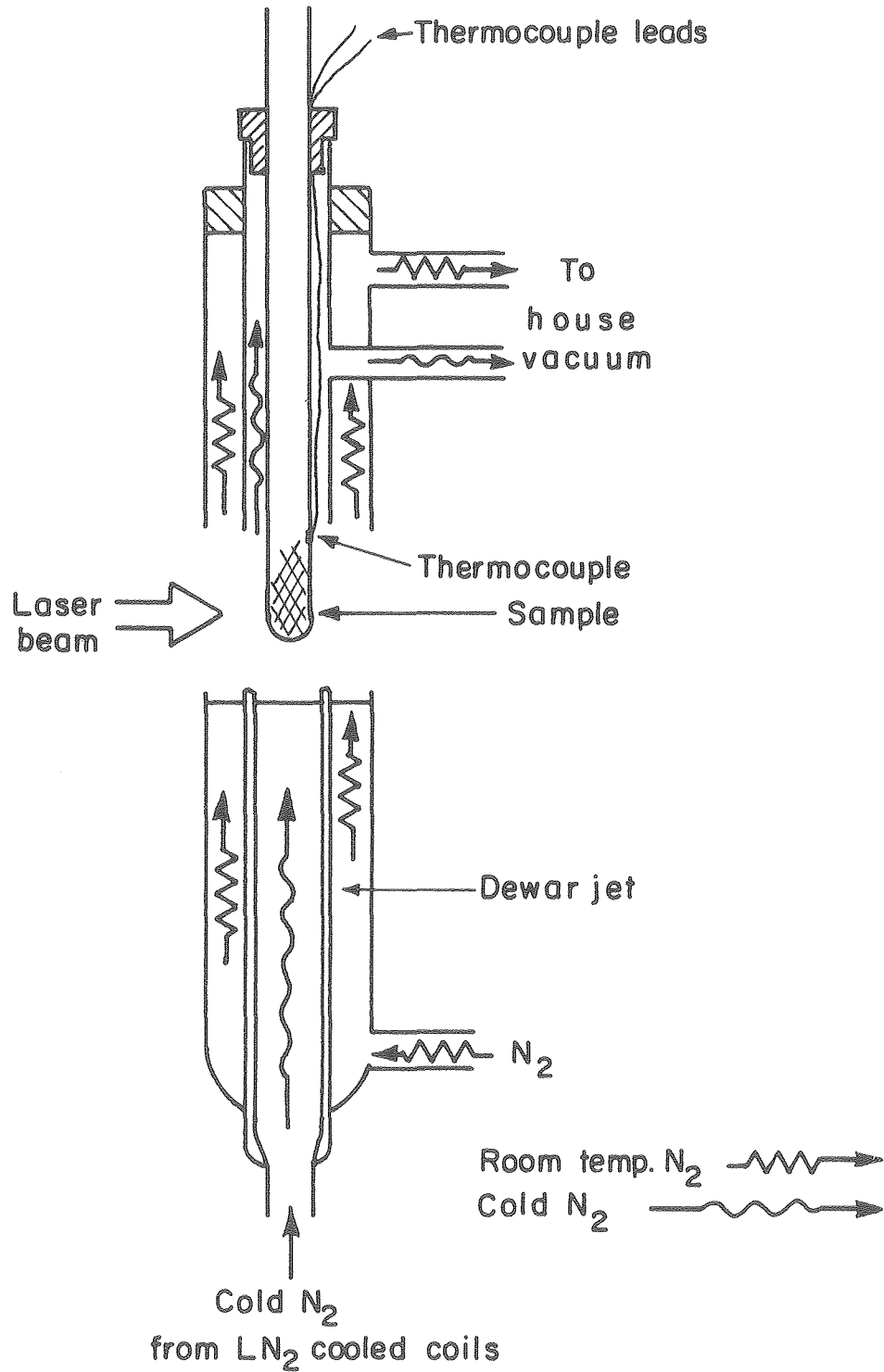
XBL 8010-6001A

Figure 1-2. Low temperature device for Raman.

XBL 8010-6006

II. $XeF_2 \cdot AsF_5$ STUDIES

A. Introduction

The 1:1 adduct of XeF_2 and AsF_5 was first prepared by Binen-boym and coworkers.[1] They characterized this material primarily on two points.

The infrared spectrum of their product pressed between silver chloride windows showed a weak band at 565 cm^{-1}, and a very strong band at 675 cm^{-1}. They assigned the 565 cm^{-1} band to an Xe-F stretch (v_2 of XeF_2 is at 557 cm^{-1}). And they attributed the 576 cm^{-1} band to an As-F stretch, but stated that it was two low to be an AsF_6^- band. They also found that solutions of $XeF_2 \cdot AsF_5$ in HF showed conductivities only slightly higher than the pure solvent. From these considerations, they concluded that $XeF_2 \cdot AsF_5$ was a molecular, possibly fluorine bridged, adduct.

Other studies of $XeF_2 \cdot MF_5$ and $XeF_2 \cdot 2MF_5$[2,3,4] adducts suggested instead that these materials should be regarded as $XeF^+MF_6^-$ and $XeF^+M_2F_{11}^-$ salts, based on spectroscopic and crystallographic evidence. Raman spectra of these products showed very strong bands between 590 cm^{-1} and 620 cm^{-1} attributable to $(Xe-F)^+$ stretches, and weaker bands below 390 cm^{-1} assigned to $Xe-F_{bridge}$ stretches. Crystallographic studies had also found that the $F_{terminal}-Xe-F_{bridge}$ unit in these materials was highly unsymmetrical.

Moreover, Sladky and coworkers[3] showed that $XeF_2 \cdot AsF_5$ lost AsF_5 readily to form $2XeF_2 \cdot AsF_5$, which had been characterized as the salt $Xe_2F_3^+AsF_6^-$. Also, preliminary Raman studies had shown no

correlation to the original infrared study. So it appeared that Binenboym et al.[1] might have been misled due to difficulties in handling this unstable material.

At the initiation of the work described in this chapter, the crystal structure of $XeF_2 \cdot AsF_5$,[7] shown in Figure 2-1, had been determined by Zalkin and coworkers from a crystal found serendipidously during an attempt to grow crystals of $(XeF)_2SO_3F^+ AsF_6^-$. However, a number of ambiguities remained. The preliminary Raman spectra obtained by Sladky[8] did not agree with that obtained by Gillespie and Landa,[4] Sladky's appearing much more similar to spectra obtained for $Xe_2F_3^+ AsF_6^-$. This suggested the remote possibility that there was also a 1:1 adduct that was actually $Xe_2F_3^+ As_2F_{11}^-$.

The purpose of the work described in this chapter was to clear up the spectroscopic and preparative uncertainties. The bonding characteristics of this material will also be discussed.

B. <u>Starting materials and reactants</u>

1. <u>Xenon difluoride</u>. XeF_2 was prepared according to the method given by Williamson[9] and characterized by its Raman spectrum.[10]

2. <u>Bromine pentafluoride</u>. BrF_5, as supplied in cylinders by Matheson, Co., (East Rutherford, N.J.) contained significant quantities of lower fluorides. These were fluorinated by heating the impure BrF_5 with fluorine in a monel can, or by exposing BrF_5 to fluorine in a quartz bulk at room temperature.

3. <u>Fluorine</u>. F_2 was obtained from Matheson.

4. <u>Arsenic pentafluoride</u>. AsF_5 was obtained from Ozark Mahoning (Tulsa, Okla.)

C. <u>Experimental</u>

1. <u>Synthesis</u>. Typically, XeF_2 (1/2 to 2 grams) was transferred in the Dri Lab into a preweighted quartz bulb joined to a brass valve. The bulb contained a Teflon coated magnetic stirring bar. Sufficient bromine pentafluoride to dissolve the XeF_2 was condensed into the bulk under vacuum. The mixture was warmed to room temperature, and exposed to gaseous arsenic pentafluoride to maintain a total pressure of one to two atmospheres for approximately one hour, during which time the solution was being mixed by the externally driven stir bar. The mixture was then cooled to $-23°C$ (CCl_4 slush bath) and excess arsenic pentafluoride and solvent pumped off slowly. The remaining product was warmed to room temperature for a brief pumping to remove the last traces of solvent.

In the best instance, .684 g (4.04 mmole) XeF_2 reacted with .688 g (4.05 mmole) AsF_5, yielding an $XeF_2:AsF_5$ ratio of 1:1.002. The product was very pale yellow.

2. <u>X-ray powder data</u>. An x-ray powder pattern of $XeF_2 \cdot AsF_5$ was desired to establish that the crystal structure determination corresponded to the bulk material. Due to the time involved in loading a capillary in the Dri Lab, and in light of the known instability of $XeF_2 \cdot AsF_5$ toward AsF_5 loss, it seemed unlikely that a power pattern of reliably pure 1:1 adduct could be obtained using the con-

ventional loading technique. A special reactor (Figure 2-2) was prepared with .5 mm capillaries attached along its neck. XeF_2AsF_5 was prepared as usual in the bottom portion of the reactor. The resultant product was then broken up and powdered using the Teflon coated magnetic stirring bar. A small amount of the powder was then tipped into one of the capillaries, which was subsequently sealed off. The x-ray powder pattern was then readily indexed on the basis of single crystal unit cell parameters. This indexing is shown in Table 2-1.

3. Preliminary Raman spectra. Early Raman spectra obtained from this material showed a pattern characteristic of the $Xe_2F_3^+ AsF_6^-$ salt. However, in one particular instance, while trying to optimize the intensity of a peak preliminary to obtaining the full spectrum, it became obvious that the peak was being bleached by the laser beam. A series of quickly run spectra over the Xe_F^- stretching region confirmed that the sample was decomposing in the beam to $Xe_2F_3^+$ AsF_6^-. This observation explained Sladky's[8] spectra. Gillespie and Landa's spectrum of $XeF_2 \cdot AsF_5$[4] also showed some of this impurity.

4. Low temperature Raman spectroscopy. After the low temperature device was built, the Raman spectrum of $XeF_2 \cdot AsF_5$ held at $-100°C$ was obtained. This spectrum was much sharper and more detailed than that obtained by Gillespie and Landa, probably due to the lowered temperature. It also shows only a small trace of $Xe_2F_3^+ AsF_6^-$

impurity. This spectrum and the spectra of $Xe_2F_3^+$ AsF_6^- and Cs^+ AsF_6^-, for comparison, are shown in Figure 2-3.

D. Discussion

1. Bond lengths. Xe-F and As-F bond lengths for $XeF_2 \cdot AsF_5$[7] and other relevant structures[11,12] are listed in Table 2-2. It is clear that both the AsF_6 and XeF_2 units are highly distorted. The average As-F$_{term.}$ bond length for $XeF_2 \cdot AsF_5$ is the same as the average bond length in molecular AsF_5. However, these bond lengths are perhaps misleading. Taking into account the vibrational motion of the fluorines about the arsenic according to the riding model,[13] the average bond length is corrected to 1.73Å. This is essentially the same as the similarly corrected As-F distance found in $Xe_2F_3^+$ AsF_6^-, which has been shown both spectroscopically and crystallographically to be nearly unperturbed octahedral AsF_6^-. This suggests that the arsenic in the 1:1 adduct is more AsF_6^--like than AsF_5-like. However, the bridging fluorine distance of the AsF_6 entity results in a substantial deviation from octahedral symmetry.

If the Xe-F$_{br.}$ distance of 2.14Å in $Xe_2F_3^{+}$[11] is taken as a standard for an unambiguous case of bridging, then the 2.21 Å found for Xe-F$_{br.}$ in the 1:1 adduct indicates a case of weaker bridging. The Xe-F$_{term.}$ distance in the 1:1 adduct is correspondingly shorter than the Xe-F$_{term.}$ bond of $Xe_2F_3^+$. Since $(XeF)^+$ is formally a single bonded species, whereas XeF_2 is formally half bonded, the shortened Xe-F bond length should be an indication of its greater $(XeF)^+$ character.

2. <u>Raman spectra</u>. The Raman spectra of $XeF_2 \cdot AsF_5$ and $Xe_2F_3^+ AsF_6^-$ show the same trends as the bond length information. The Xe-F$_{term.}$ stretches for the 1:1 adduct are at higher energy than the corresponding stretches for $Xe_2F_3^+$. Gillespie and Landa[4] assign the 417 cm^{-1} and 400 cm^{-1} bands of $Xe_2F_3^+ AsF_6^-$ to Xe-F$_{br.}$ stretches. If this assignment is correct, then the assignment of the 346 cm^{-1} band to the Xe-F$_{br.}$ stretch of $XeF_2 \cdot AsF_5$ is consistent with the bridge weakening indicated by the longer bond length. However, this stretching frequency, compared to 492 cm^{-1} for the symmetric stretch of XeF_2, indicates that the bridge is still very significant.

Interpretation of the As-F bands is less straightforward. There is no reliable assignment for a unique As-F$_{br.}$ stretch. Gillespie and Landa[4] assigned a band at 443 cm^{-1} in their spectrum to this, but that band is not observed here.

What is more significant is the pronounced deviation from octahedral symmetry present in the 1:1 adduct. For octahedral symmetry, only ν_1 (A_{1g}), ν_2 (E_g), and ν_5 (F_{2g}) are allowed in Raman spectra. But for $XeF_2 \cdot AsF_5$, ν_3 (F_{1u}) is clearly visible, and is split into essentially two bands, consistent with a decline in symmetry from O_h to approximately C_{4v}. The ν_5 band is similarly split and the allowed ν_2 band is no longer evident. These considerations indicate that the AsF_6 entity in the structure should be considered an octahedron only as a first approximation.

3. <u>Overall packing considerations</u>. In general, there is a tendency for AsF_6^- salts to be isostructural with PF_6^- salts, but different

from RuF_6^- and SbF_6^- salts.[7] The As/P system prefers 6:6 (NaCl-type) coordination, while the Ru/Sb system prefers 8:8 (CsCl-type) coordination, and this preference can be related to the relative polarizabilities of the anions.

The structural unit in $XeF_2 \cdot AsF_5$ is very similar to that found for $XeF_2 \cdot RuF_5$,[5] but the overall packing of the formula units is different. In particular, the XeF unit in the arsenic compound is surrounded by six AsF_6 units, while the XeF unit in the ruthenium compound is surrounded by eight RuF_6. This suggests that the XeF .MF adducts have sufficient ionic character for this factor to dictate their packing arrangements. Therefore, their formulation as $(FXe)^+ MF_6^-$ is meaningful.

4. <u>Interpretation</u>. The characterization of $XeF_2 \cdot AsF_5$ as either primarily an ionic species or primarily a bridged (covalent) species is unavoidably ambiguous. The structure and spectroscopy indicate strong contributions from both bonding types.

Ultimately, the best judgment of any model is its predictive ability rather than its interpretive ability. From this consideration, the two models are probably of equal value. The ionic model predicted the overall packing correctly, and in particular, the difference between $XeF_2 \cdot AsF_5$ and $XeF_2 \cdot RuF_5$, which one would otherwise anticipate to be structurally more similar. However, the molecular model predicted the conductivity behavior of $XeF_2 AsF_5$ solutions that Binenboym and coworkers[1] reported. But since the structure in solution is not necessarily the same as the structure in the solid, where the Madelung term would favor ionic character, this datum does not by itself contradict the ionic model.

5. <u>Summary</u>. For the adduct $XeF_2 \cdot AsF_5$, spectroscopic and structural considerations suggested that it is truly intermediate between the fluorine bridged molecular adduct $FXeFAsF_5$, and the salt $XeF^+AsF_6^-$. Neither model is by itself sufficient.

REFERENCES

1. J. Binenboym, H. Selig and J. Shamir, J. Inorg. Nucl. Chem., 30 (1968) 2863.

2. N. Bartlett, Endeavour, 31 (1962) 107.

3. F. O. Sladky, P. A. Bulliner, and N. Bartlett, J. Chem. Soc. A (1969) 2179.

4. R. J. Gillespie and B. Landa, Inorg. Chem., 12 (1973) 1383.

5. N. Bartlett, M. Gennis, D. D. Gibler, B. K. Morrell, and A. Zalkin, Inorg. Chem., 12 (1973) 1717.

6. V. M. McRae, R. D. Peacock, and D. R. Russell, Chem. Commun. (1969) 62.

7. The work presented here was included as a portion of the crystal structure report: A. Zalkin, D. L. Ward, R. N. Biagioni, D. H. Templeton, and N. Bartelett, Inorg. Chem., 17 (1978) 1318.

8. F. O. Sladky, unpublished.

9. S. M. Williamson, Inorg. Syn., 11 (1968) 147.

10. D. L. Smith in "Noble Gas Compounds," H. H. Hyman, ed., p. 295, The University of Chicago Press, Chicago and London, 1963.

11. N. Bartlett, B. G. DeBoer, F. J. Hollander, F. O. Sladky, D. H. Templeton, and A. Zalkin, Inorg. Chem., 13 (1974) 780.

12. F. B. Clippard, Jr., and L. S. Bartell, Inorg. Chem., 9 (1970) 805.

13. W. R. Busing and H. A. Levy, Acta. Cryst., 17 (1964) 142.

Table 2-1. X-ray powder data for XeF_2,AsF_5

	$1/d^2$		
hkℓ	calc.	obs.	Rel. intensity
002	.0161	.0170	vw
11$\bar{1}$	.0518	.0515	s
111	.0588	.0586	s
004	.0642	.0648	s
	----	.0706	vvw
112	.0744	.0774	m
11$\bar{3}$	.0768		
014	.0896	.0885	vw
113	.0980	.0988	mw
020	.1016		
021	.1056		
20$\bar{2}$	.1056	.1080	m
105	.1086		
120	.1275	.1241	w
12$\bar{1}$	.1280		
11$\bar{5}$	.1340	.1347	w
121	.1350		
023	.1376	.1396	w
20$\bar{4}$	.1396		
212	.1592	.1599	w

(continued)

Table 2-1. (Continued)

hkℓ	calc.	obs.	Rel. Intensity
		$1/d^2$	
024	.1658	.1679	w
11$\bar{5}$	.1693		
204	.1961	.1970	w
10$\bar{7}$	.1979		
220	.2052		
20$\bar{6}$	.2058	.2059	w
124	.2059		
216	.2312	.2349	w
22$\bar{4}$	.2412	.2426	w
13$\bar{1}$	.2549	.2550	mw
008	.2570		
131	.2620	.2635	mw
31$\bar{3}$	.2629		
133	.3012	.3077	w
315	.3059	.3077	w
20$\bar{8}$	.3041		
11$\bar{9}$	.3447	.3484	vw
040	.4062	.4090	w
119	.4083		

Table 2-2. Bond lengths of $XeF_2 \cdot AsF_5$ and
related structures

$XeF_2 \cdot AsF_5$ [7]

As–F$_{\text{term.}}$ (ave)	1.68	(1.73)
As–F$_{\text{br.}}$	1.81	(1.84)
Xe–F$_{\text{br.}}$	2.21	
Xe–F$_{\text{term.}}$	1.87	

AsF_5 [12]

As–F (ave)	1.68

$Xe_2F_3^+$ AsF_6^- [11]

Xe–F$_{\text{term.}}$	1.90	
Xe–F$_{\text{br.}}$	2.14	
As–F (ave)	1.63	(1.74)
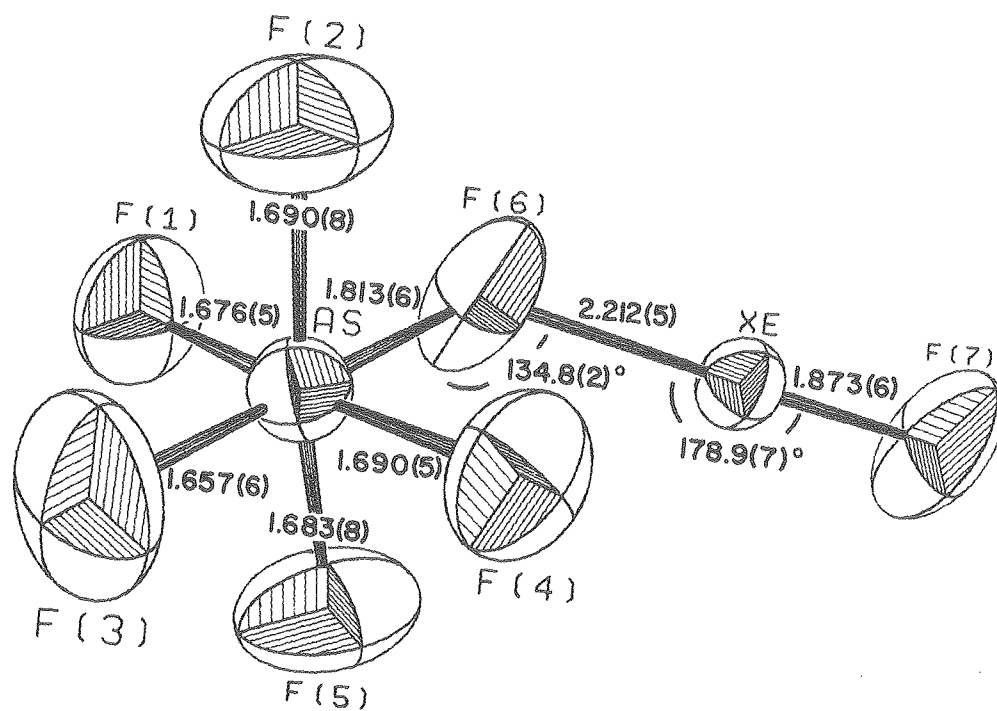
Figure 2-1. XeF$_2$·AsF$_5$.
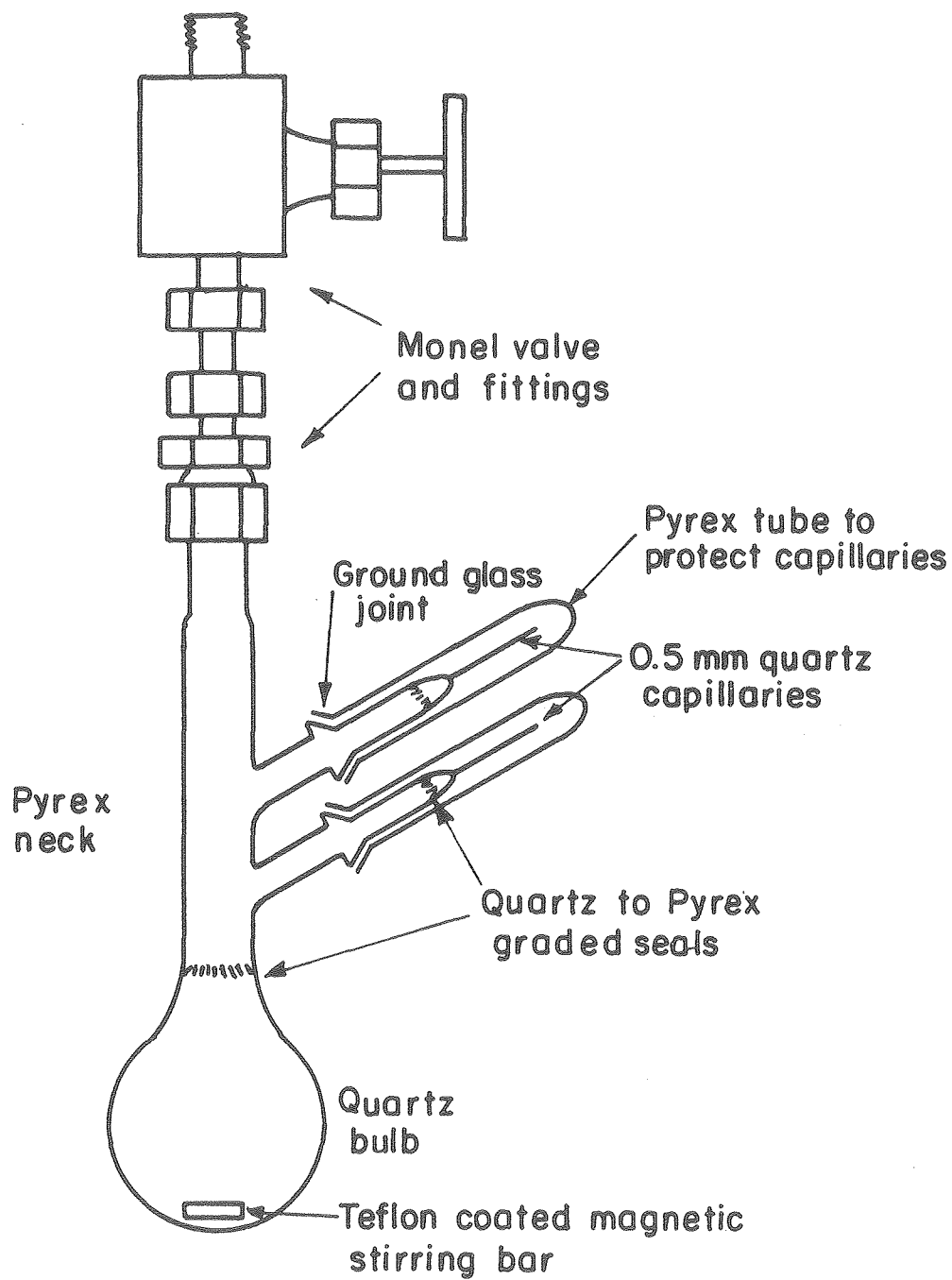
Figure 2-2. Reactor for preparing $XeF_2 \cdot AsF_5$ powder sample.

23
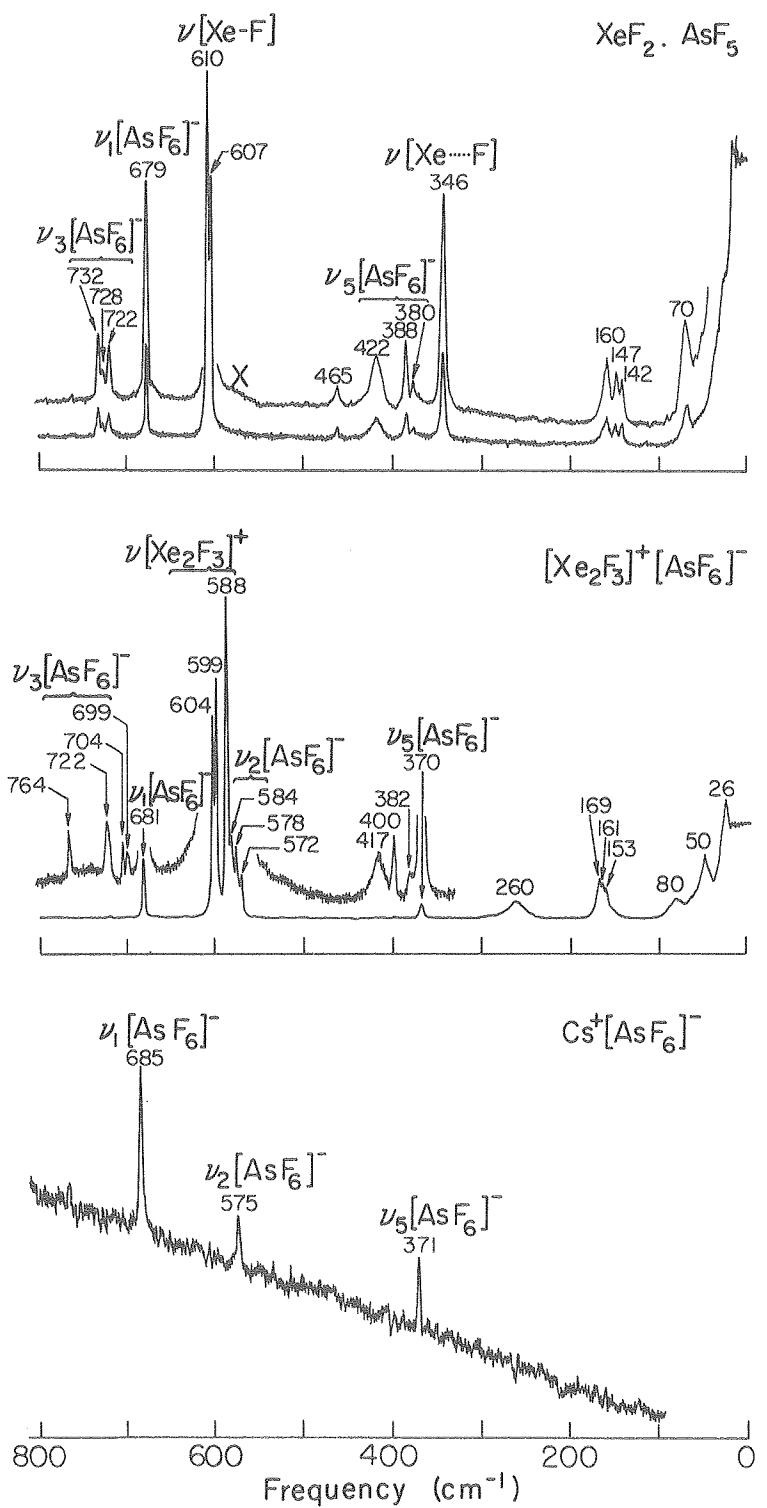
Figure 2-3. Raman spectrum, T = -100°C.

III. PREPARATION AND CHARACTERIZATION OF
GRAPHITE FLUOROSULFATES

A. Introduction

1. General Background. Graphite,[1] the more stable allotrope of carbon, is a layered material characterized by strong bonding within the planes, but with weak interactions between adjacent planes. An individual layer can be viewed as an infinite delocalized system, with sp^2 hybridized carbons forming a flat, hexagonal sigma-bonded network, while the remaining p orbitals perpendicular to the plane form an extended pi system. Interactions, between layers, though weak, are sufficient to induce long range order. α-graphite, the most stable form (Figure 3-1a) shows an abab stacking arrangement; in β-graphite (Figure 3-16) the stacking arrangement is abcabc. Also common is a turbostatically disordered system, which shows no long range order in the stacking, with a slightly larger interlayer spacing.

Electrically, graphite is a semimetal. The room temperature basal plane conductivity for single crystals of natural graphite is approximately 2500 $(ohm-cm)^{-1}$, or about one-twentieth that of copper. Perpendicular to the basal plane, the conductivity is much lower. The temperature dependence of the conductivity is metallic. The conductivity is attributed to the valence and conduction bands overlapping, so that both holes in the former and electrons in the latter contribute to the conductivity.

Intercalation compounds[2] of graphite form a class of materials formed by the insertion of guest species between some or all of the graphite layers. The space between adjacent layers is referred to as a gallery. If each gallery is occupied, the compound is first stage. If every other gallery is occupied, the compound is second stage, and so on. Both guests that are regarded as electron withdrawing (e.g., $SO_3F + e^- \rightarrow SO_3F^-$) and electron donating (e.g., $K \rightarrow K^+ + e^-$) can be introduced. Only the former type will be considered here.

The feature of these materials that has drawn the most interest is their markedly increased conductivity relative to the parent graphite. Generally, this is attributed to electron withdrawal from the valence band to create a larger number of conducting holes. However, the extent of formal oxidation by guests, and the details of its effect on conductivity, are subjects of considerable debate.

A system frequently studied by other workers has been the graphite plus arsenic pentafluoride system, where the extent of formal oxidation has not been resolved. Several workers[3] have argued that the formal oxidation is slight, while Bartlett and his coworkers[4] argue for the formal oxidation according to the classical reaction of AsF_5:

$$3AsF_5 + 2e^- \rightarrow 2 AsF_6^- + AsF_3.$$
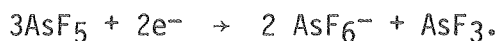
The addition of fluorine to C_8AsF_5 to yield C_8AsF_6 leads to a decrease in conductivity despite the inarguable increase in formal

oxidation. The conductivity of this fluorinated material is similar to that found for the first stage materials C_8MF_6 (M = Os, Ir), where magnetic susceptibility[4c] measurements have shown the guests to be the monocharged anion. This result indicates that at sufficiently high formal oxidation, charge localization ensues, reducing electron mobility. Others suggest that some fluorination of the graphite lattice would also lower the conductivity. Both charge localization and graphite fluorination could result in structural changes detectable in x-ray diffraction studies.

Chemically characterizing the state of the guest species is a particularly difficult problem. Normal techniques such as infrared and Raman spectroscopy are not easily applicable because these materials are opaque and highly reflective to the radiation. Magnetic susceptibility measurements[4a,4c] have provided some information for systems involving metal hexafluorides, but there are generally no magnetic species expected in systems employing arsenic fluorides or fluorosulfate. Single crystals of graphite, scarce to begin with, generally do not maintain their integrity upon intercalation, so that detailed structural information is not readily obtainable. Therefore, less direct approaches have been employed here in an attempt to characterize some of these materials.

The work considered here deals mostly with graphite fluorosulfates. Ubbelohde[5] et al. prepared the first example of this system by electrochemical oxidation in fluorosulfonic acid at a graphite anode.

This produced a first stage material, but difficulties in handling the product prevented any detailed analysis.

The graphite fluorosulfate system is formally analogous to the graphite bisulfate system.[5,6] The latter materials have generally been prepared in sulfuric acid solutions, with oxidation achieved either anodically, or chemically by an agent such as HNO_3. The electrochemically produced graphite bisulfate showed an overall stoichiometry of roughly $C_7(HSO_4^-,H_2SO_4)$,[5,6c] but the current required to produce this material corresponded to a charging of only C_{23}^+, requiring that for each HSO_4^-, there were 2.5 H_2SO_4. Charging of roughly C_{24}^+ is also observed for a number of other graphite $C_x^+A^-yHA$ systems prepared electrochemically in the appropriate acids.[5,6c,7]

The recurrence of C_{24}^+ as the ultimate charging for these systems appears to be a consequence of the potential required to further oxidize the graphite exceeding the potential required to generate peracid species or oxygen.[5] There appears to be no reason why a higher charge than C_{24}^+ could not be obtained for salts free of the protonic acid. For mineral acid systems, it seems that the concentration of anions in the graphite salt is determined by the graphite charge attainable, and that the concentration of mineral acid is determined by the remaining space in the galleries.

The synthetic approaches employed here should produce unique materials, since the limiting factor of synthesizing in excess acid, and the complication factor of requiring a foreign oxidizing agent, can be avoided. The fluorosulfates in this work were formed by chemi-

ical oxidation with peroxydisulfuryldifluoride, $S_2O_6F_2$, first synthe-sized by Dudley and Cady.[8] $S_2O_6F_2$, a convenient oxidative fluorosulfon-ating agent,[9] is a liquid at room temperature, with a vapor pressure sufficient for facile transport through a vacuum line. Its reduction product is the fluorosulfate anion. Despite its power as an oxidizing agent, $S_2O_6F_2$ is a poor fluorinating agent, so the possibility of fluorinating graphite in this system is slight. However, the aspect of the fluorosulfate work that seemed most promising was the possibil-ity of producing materials that also contained controlled amounts of fluorosulfonic acid, allowing a study of materials with very similar structures but greatly varying degrees of formal oxidation.

2. Experimental approaches and procedures

Acid-free first-stage graphite fluorosulfates were prepared by the direct interaction of excess $S_2O_6F_2$ (either vapor or liquid) with graphite. Two approaches were employed in attempts to make higher stage materials. One technique involved limiting the total amount of the peroxide exposed to the graphite (reactant limited); the other in-volved regulating the vapor pressure of the peroxide (pressure limited).

First stage graphite fluorosulfates which also contained acid were generally prepared by addition of appropriate amounts of acid and per-oxide to graphite. However, due to the inconveniences of this approach, indirect methods of introducing acid to the system were also attempted. These involved in situ production of HSO_3F in the interaction of $S_2O_6F_2$ or graphite fluorosulfate with a hydrogen donor.

Most of the work here employed powdered graphite. Some attempts were made to react large pieces of graphite, particularly for some diffractometer studies. These preparations will be described in the next chapter.

Generally, stoichiometries were assessed by both gravimetry and conventional carbon analysis. Gravimetry was complicated by the possible interaction of the rather aggressive reactants used here with the reaction vessels, particularly with metal valves. Small quantities of graphite were generally employed (often in the 100 mg range), so spurious weight changes could have serious effects on the calculated stoichiometries.

While carbon analysis was at first considered to be a good check on composition, this technique also proved to be unreliable at times. In particular, graphite does not always burn completely under normal analysis conditions. This was particularly true of pure graphite, where samples of HOPG (highly ordered pyrolytic graphite, which will be described in the next section) analysed under normal conditions gave carbon percentages as low as 42%. A combination of V_2O_5 catalyst and prolonged burning time (two minutes) seemed to minimize the problem. In general, the problem was not nearly as severe with the reacted samples, and NASA graphite (another type of graphite, described in next section) compounds were less affected than HOPG samples.

Samples for analysis were held in either pyrex bottles or FEP tubes, which were in turn enclosed in Schlenck tubes. The analysis

laboratory's normal procedure for handling air sensitive materials was to transfer them into a helium filled glovebox, and there load them into crimp-sealed aluminum capsules. In the early stages of this work, the high corrosiveness of some of these materials was not realized, so the time period between when the sample was loaded into the bottle to the time it was actually loaded into the aluminum capsule could have had a serious impact on the reported analysis.

B. Starting materials and reactants

1. Graphites. Two types of graphite were employed during the course of these studies. NASA graphite (so called because it was originally produced for the space agency for use as a heat shield material for reentry vehicles) is a moderately ordered pyrolytic graphite. X-ray powder photographs show this material to be turbostatically disordered (c = 3.42 Å, a = 2.457 Å) with only diffraction lines corresponding to hk0 and 001 reflections observable. Although this material was nominally pure carbon, it developed a surface coating (probably hydroxyl groups) when exposed to air. The extent of this problem was not realized at first. Eventually, the following procedure was used to prepare clean, dry powdered graphite.

The desired quantity of graphite was cut to a fine powder using a file, and then passed through a sieve to remove any large chips. The powdered graphite was transferred to a quartz tube and heated to a red glow under vacuum until most gas evolution had stopped. After cooling, the graphite was exposed to increasing pressures of fluorine, starting at about fifty torr and raised slowly to approximately

one atmosphere. The fluorine was then pumped off. The initial introduction of fluorine to the graphite resulted in substantial heat generation, and if care was not taken to introduce the fluorine very slowly, the graphite would ignite. However, once passivated in this manner, further addition of fluorine caused no heat generation. The passivated graphite was then heated to a red flow under vacuum. Sufficient material for several experiments was prepared at one time and stored in the Dri Lab. X-ray powder patterns of the treated material were identical to those of the untreated material.

NASA graphite was readily available during the entire course of this work, and was used for the bulk of these studies.

Highly ordered pyrolytic graphite (HOPG) was provided by Dr. Arthur Moore of Union Carbide (Carbon Products Division, Parma, Ohio). It is essentially ordered microcrystalites of predominantly α-graphite, with some β-graphite present, where the c-axes of the crystallites are very nearly parallel ($\pm 1/2°$), while the a-axes are randomly oriented. Some samples also showed some turbostatically disordered graphite. Tablets could be cut and cleaved to a specific size, or powder could be cut with a file. In each case, the sample was heated to a red glow under vacuum before reaction.

Due to its limited availability, HOPG was used only for a few experiments during the later phases of this work.

X-ray powder patterns for the two types of graphite, illustrating their relative degrees of order, are shown in Figure 3-2, and their measurements listed in Table 3-1.

2. $\underline{SO_3 \text{ and } HSO_3F}$ were obtained from Allied Chemical Co. (Morris-town, N.J.). SO_3 was transferred into Pyrex storage bottles provided with Kontes valves, and BF_3 was added as a stabilizer. HSO_3F was distilled under vacuum to either Pyrex vials or Pyrex storage bottles with Kontes valves.

3. $\underline{S_2O_6F_2}$ was prepared via two routes involving the decomposition of $Xe(OSO_2F)_2$, prepared according to the following reactions:[10]

$$XeF_2 + 2\ HSO_3F \rightarrow Xe(OSO_2F)_2 + 2\ HF$$
$$XeF_2 + 2\ SO_3 \rightarrow Xe(OSO_2F)_2$$
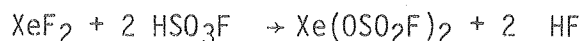
The xenon fluorosulfate was then decomposed to yield xenon, which was recovered, and $S_2O_6F_2$. The distilled product, shown to be pure by Raman spectroscopy,[11] was stored in dry Pyrex or quartz bottles with stainless steel valves and fittings.

4. $\underline{\text{Perfluoro tert-butyl alcohol}}$ (PFTBA), obtained from P.C.R. (Gainesville, Fl.), was distilled into a pyrex bottle provided with a Kontes valve.

5. $\underline{HCl \text{ and } CHF_3}$ were obtained from Matheson.

C. Experimental

1. Preparation of acid free first stage graphite fluorosulfate from NASA graphite. Pretreated graphite was loaded into a preweighed passivated reactor consisting of a stainless steel valve joined to a quartz tube via stainless steel fittings and Teflon ferrules. A Pyrex wool plug was inserted into the top of the tube to prevent powder from being

sucked past the valve during evacuation. The tube was evacuated and reweighed to determine the amount of graphite present. Excess $S_2O_6F_2$ was then added, either as a vapor or as a liquid, and allowed to react at ambient temperature for at least one hour. When vapor was reacted with graphite at room temperature, the reaction vessel became warm to the touch. Excess peroxide was then pumped off, and the reactor reweighed to assess fluorosulfate uptake.

This procedure yielded a dark blue, moderately reflecting solid product. Gravimetry and carbon analysis gave the composition C_xSO_3F, where $7.1 \leqslant x \leqslant 7.8$. X-ray powder photographs yielded a c-spacing of 7.60 to 7.70 A. Two sets of lines were always observed. One was associated with the in-plane hexagonal network of the carbons, corresponding to the 100 and 110 reflections of graphite. The other was associated with the c-spacing. The 002 reflection was by far the strongest, with 001, 003, and sometimes 004 also visible. Samples prepared from large excesses of liquid $S_2O_6F_2$ generally showed extra lines, the relative intensity of which varied from sample to sample. These were not interpreted.

Checks by infrared spectroscopy of the vapors over the reaction mixture showed $S_2O_6F_2$ and small quantities of SiF_4 and $S_2O_5F_2$. The graphite products were stable to overnight pumping at room temperature. To test to see if $S_2O_6F_2$ could be driven out, a sample held in a quartz tube was heated vigorously. Little gas evolution, as detected by a thermocouple gauge, was detected until the sample flashed, generating sufficient vapor for an infrared spectrum. The

infrared showed only SO_2F_2 and SiF_4, and neither $S_2O_6F_2$ nor $S_2O_5F_2$.

Samples could be stored in dry Pyrex bottles for short periods of time. But after a few weeks the bottles would inevitably show etching, and x-ray powder patterns of the stored material showed an enlarged c-spacing. Passivated FEP liners inside the bottles, separating the sample from direct contact with the glass, seemed to prevent this sample degradation.

2. Preparation of higher stages of acid free NASA graphite fluorosulfate by reactant limitation. A powdered graphite sample was loaded into a reactor of the type described in the preceding section. An approximately 100 cc bulb was filled with $S_2O_6F_2$ vapor to the pressure appropriate to the desired stoichiometry, and this exposed to the graphite. However, early results showed that this resulted in the formation of some first stage material and left some unreacted graphite, based on x-ray powder photographs. A more satisfactory approach involved cooling the premeasured peroxide with a dry-ice temperature bath held in an ordinary beaker. The slow increase of $S_2O_6F_2$ vapor pressure as the bath warmed allowed for a slower, more even reaction. An additional measure to achieve homogeneous reaction involved maintaining the reaction bulb in a horizontal orientation, allowing a greater surface area of graphite to be exposed. The bulb could be rotated periodically during the course of the reaction to expose fresh surfaces.

Under these conditions, a new material, phase B, was observed. When the stoichiometry was adjusted to approximately $C_{12}SO_3F$, pure phase B was obtained. Samples richer in fluorosulfate showed some first stage product; material poorer showed unreacted graphite. X-ray powder patterns of this material showed only one line not attributable to the graphite lattice, with d = 3.6 Å. Using NASA graphite, no other phases were ever observed. The first stage impurities sometimes observed had a c-spacing of 7.6 Å.

3. <u>Preparation of higher stage graphite fluorosulfates by pressure limitation.</u> Attempts were made to prepare higher stages of graphite fluorosulfate by regulating the pressure of the $S_2O_6F_2$ presented to the graphite, using the type of reaction setup used for making first stage materials. Vapors from $S_2O_6F_2$ held at $-45°C$ (chlorobenzene slush) or $-30°C$ (bromobenzene slush), where its vapor pressures were approximately 1 and 4 torr respectively, were allowed to react with graphite samples. The x-ray powder pattern of the material exposed to 4 torr $S_2O_6F_2$ showed some first stage product and unreacted graphite in addition to phase B. The product of the 1 torr reaction showed only one line not attributed to graphite, with d = 3.7 A.

4. <u>Preparation of acid containing first stage NASA graphite fluorosulfates by direct methods.</u> Graphite samples were held in reactors made by drawing down and rounding one leg of a glass Kontes valve. Distilled HSO_3F was held in a similar tube. The two were joined via a T-union, with the third port of the union going through a valve to vacuum.

When graphite fluorosulfates, either pure first stage or mixtures of first stage and phase B, were exposed to fluorosulfonic acid, pure first stage materials usually resulted, with c-spacings larger than those expected for the acid-free analogs. When mixtures of graphite and graphite fluorosulfate were exposed to the acid, a mixture of first stage and phase C usually resulted, where phase C appears to be an acid-containing analog of phase B. The results of these reactions are listed in Table 3-2. Infrared spectra of the vapors over the reaction mixture show small amounts of SiF_4 and $S_2O_5F_2$. While this approach could produce first stage products, the amount of fluorosulfonic acid actually incorporated could not be determined.

In one instance, an acid containing material, c = 7.84 Å, was treated with $S_2O_6F_2$. The product showed a c-spacing of 7.78 Å.

5. First stage acid containing NASA graphite fluorosulfate by stoichiometric synthesis. The most successful approach to production of these materials in large quantities involved adding stoichiometric amounts of HSO_3F and $S_2O_6F_2$ to graphite samples. A reactor of the type shown in Figure 3-3 was used. In the Dri Lab, graphite was loaded into the reactor. HSO_3F was condensed onto the sample through the Kontes valve, and then the reactor reweighed. The amount of $S_2O_6F_2$ required to yield a first stage material was then calculated, and an amount slightly in excess of that measured out in the 100 cc ballast and then admitted into the reactor through the metal valve. When the reaction was complete (judged by the mixture becoming a free-flowing powder), the sample was pumped down via the protected metal valve.

The products of these preparations were very reflective, blue, free-flowing powders that were stable to dynamic vacuum at room temperature. If stored in pyrex bottles, etching was evident within one day, but FEP liners appeared to protect sample integrity. The agreement between gravimetry and analysis was often poor, suggesting that some of the observed weight uptake was associated with attack on the reactor, despite pre-passivation of the reactor. The results of these preparations are listed in Table 3-3.

6. <u>Hydrogen abstraction reactions with NASA graphite fluorosulfate.</u>
The purpose of the hydrogen abstraction reactions study was to find a system in which C_xSO_3F would react cleanly and quantitatively with a hydrogen donor to yield an acid containing fluorosulfate with the same overall fluorosulfate composition of the starting material. This would allow for a comparison of the two materials solely as a function of hydrogen content (and hence charge) without the complication of stoichiometry variations and uncertainties for different preparations.

Chosen as reactants were H_2, CHF_3, $(CF_3)_3COH$ (perfluorot-butyl alcohol, PFTBA), and HCl. H_2 was chosen as the simplest system possible. Palladium metal was chosen as a catalyst for this reaction, since H_2 dissolves in it atomically. The others were chosen based on their reactivity as H° donors toward $S_2O_6F_2$. The anticipated reactions, assuming H° abstraction, were:

$$C_x^+SO_3F + yH_2 \rightarrow C_x^{+(1-2y)}(SO_3F, HSO_3F)$$

$$C_x{}^+SO_3F + yHA \rightarrow C_x{}^{+(1-y)}(SO_3F, HSO_3F) + A^\circ$$
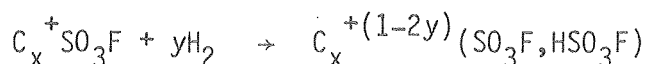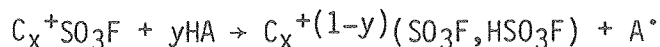
with the various A° reacting further:

$$2\ CF_3{}^\circ \longrightarrow C_2F_6$$

$$(CF_3)_3CO^\circ \rightarrow (CF_3)_2CO + CF_3{}^\circ \ (etc)$$

$$2\ Cl^\circ \longrightarrow Cl_2.$$
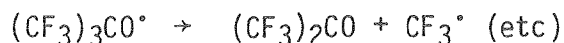
First stage graphite fluorosulfate was exposed to each reactant. Hydrogen was added in large excess. Other reactants were added in sufficient quantity to convert roughly one half of the available fluorosulfate to acid. The reactions were assessed by observing either the x-ray powder pattern of the product, infrared spectra of the vapors over the reaction mixture, or both. The results of these reactions are summarized in Table 3-4.

7. Preparation of acid containing NASA graphite fluorosulfates by in situ generation of HSO_3F. The purpose of this study was to find a method of producing products of controlled SO_3F and HSO_3F composition. The advantage of this approach was that the hydrogen sources used were much more readily handled and easily measured than HSO_3F. Both HCl and PFTBA are volatile and non-reactive (relative to other reagents employed here), in contrast to the highly corrosive, low volatility HSO_3F. Small amounts of these materials could readily be measured out using pressure-volume techniques, and then a stoichiometric amount of $S_2O_6F_2$ added to yield a compound of known composition.

HCl and PFTBA are known to undergo hydrogen abstraction reactions with $S_2O_6F_2$, according to Kirchmeier and Shreeve:[13]

$$2\ HCl + S_2O_6F_2 \rightarrow 2\ HSO_3F + Cl_2$$

$$(CF_3)_3COH + S_2O_6F_2 \rightarrow HSO_3F + CF_3OSO_2F + (CF_3)_2CO$$
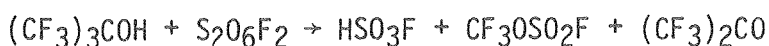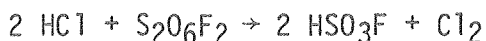
These authors reported finding only 94% of the expected Cl_2 in the HCl reaction, so this reaction was not considered ideal, but tolerable considering the other uncertainties in the measurements.

Stoichiometric amounts of $S_2O_6F_2$ and either HCl or PFTBA, sufficient to convert roughly half the incorporated SO_3F to HSO_3F, were condensed onto a graphite sample and allowed to react. The PFTBA reaction yielded a first stage product with c = 7.75 A. The infrared showed $(CF_3)_2CO$ and CF_3OSO_2F as expected, but also other peaks which could not be identified. The HCl reaction yielded first stage products with c = 7.80-7.82 Å. The infrared showed SiF_4 and $S_2O_5F_2$ over the reaction mixture.

8. Interaction of acid free and acid containing first stage NASA graphite fluorosulfates. In a preliminary experiment, x-ray powder photography showed that mixing acid-containing and acid-free fluorosulfates of NASA graphite produced a homogeneous product. To determine whether there was a smooth change in c-spacing as a function of hydrogen ion concentration, or whether there was evidence of distinct phases, two starting materials were prepared. "A" was acid free, composition by analysis $C_{7.0}SO_3F$, with c = 7.70 Å. "B" contained acid, with composition $C_{7.8}(SO_3F, HSO_3)$ by analysis, $C_{6.7}(SO_3F, HSO_3F)$ by gravimetry. The gravi-

metry suggested that the fluorosulfate content was 59–61% HSO_3F. The c-spacing of this material was c = 7.88 Å.

A series of mixtures of varying A:B ratios was prepared in passivated FEP tubes. Each mixture was then loaded into two capillaries. These capillaries had been heated strongly under vacuum, and then treated with fluorine. The loaded, sealed capillaries were in turn sealed off in pyrex tubes and stored under liquid nitrogen. This precaution was needed because of the observation that the c-spacing of this type of sample held in a capillary changed with time. The samples were kept cold prior to x-ray photography.

The plot of the observed c-spacings as a function of composition is shown in Figure 3-4. The c-spacing shown is actually based on double weighting of the 003 reflection. The breadth and curvature of the 002 relfection made it unreliable for precise measurements. The 003 was generally relatively strong and sharp in all photographs. The higher angle lines were often very weak, if observable at all, and were difficult to measure precisely. Also plotted is the a-spacing of the graphite lattice.

9. <u>First stage HOPG fluorosulfate</u>. The experimental procedures used to make first-stage NASA graphite fluorosulfate were tried. When HOPG was exposed to $S_2O_6F_2$ vapor or liquid at room temperature, there was an exothermic reaction resulting in a reflective blue product. This product was always a mixture of first and second stage materials. Heating the reaction tube to circa 80°C while the HOPG was exposed to $S_2O_6F_2$ did not yield a pure first stage material. Pumping on the product at room temperature resulted in no weight change.

In order to increase the activity of the $S_2O_6F_2$, the system was heated and for this a small volume (ca. 3cc) monel reactor was used. The reactor was fabricated from a 3/8 inch diameter monel rod which was drilled out to a wall thickness of .79 mm (1/32 inch). This was fitted to a monel Whitey valve via a monel reducing union. For the conditions intended here, 80°C warming, the vapor pressure of $S_2O_6F_2$ was calculated to be approximately two atmospheres, so Teflon ferrules could be used. Passivation was accomplished by condensing a small quantity of $S_2O_6F_2$ into the reactor, and then heating it to approximately 80°C before evacuating it. Graphite was loaded into the reactor and excess $S_2O_6F_2$ was condensed in. The entire body of the reactor was then submerged in a warm water bath at 75°C for at least an hour and a half. The excess $S_2O_6F_2$ was then pumped off, slowly at first, to avoid ejecting solids from the reactor. Two runs of this reaction each gave the stoichiometry $C_{7.0}SO_3F$, with c-spacings very near 7.7 A.

Table 3-5 summarizes the results of the HOPG plus excess $S_2O_6F_2$ reactions. Table 3-6 lists the indexing of a pure first stage HOPG fluorosulfate.

10. <u>Second stage HOPG fluorosulfate.</u> The behavior of the HOPG plus $S_2O_6F_2$ reaction suggested that second stage material might be prepared by admitting the $S_2O_6F_2$ very slowly so that local heating could be avoided. An attempt was made using an approach similar to that employed for making phase B (NASA graphite) fluorosulfate, except that excess $S_2O_6F_2$ was used. Graphite powder was exposed to $S_2O_6F_2$ held initially at -78°C. As the cold bath slowly warmed, the graphite was subjected to increasingly

higher pressures of $S_2O_6F_2$. After the $S_2O_6F_2$ had been at room temperature for several hours, the excess was pumped off. The stoichiometry by gravimetry was $C_{13.0}SO_3F$; by analysis, $C_{13.6}SO_3F$. The powder pattern indexing is listed in Table 3-7. It shows that the product is primarily second stage, with the first stage as a minor component.

11. <u>Reaction of HOPG fluorosulfate with HSO_3F</u>. 89 mg of a graphite fluorosulfate sample that was a mixture of first and second stage, with overall composition $C_{8.8}SO_3F$ by analysis and $C_{8.9}SO_3F$ by gravimetry, was loaded into a reactor of the type shown in Figure 3-2. 39 mg HSO_3F was condensed onto this, and allowed to react at room temperature for approximately forty minutes, after which the excess was pumped off. The observed weight increase was 19 mg, indicating a stoichiometry $C_{6.1}SO_3F$ by gravimetry; analysis gave $C_{7.8}SO_3F$. The x-ray powder pattern of this reflective blue product, listed in Table 3-8, indicated that this was a pure first stage compound, with c = 8.04 Å.

12. <u>Interaction of acid free and acid containing HOPG fluorosulfates</u>. Approximately equal quantities of first stage HOPG fluorosulfate (c = 7.70 Å) and acid fluorosulfate (c = 8.04 Å) were mixed. An x-ray powder pattern of this mixture showed two phases. There was a very strong set of lines corresponding to a first stage material with c = 8.00 Å. The second set of lines, whose streaky character indicated that they were dominated by reflections from some of the larger particles in the powder, could not be measured accurately, but did indicate a first stage material with c < 7.9 Å. A powder pattern of the same material taken several days later showed very little change.

D. Discussion

1. First stage graphite fluorosulfates. Several observations should be considered in identifying the species incorporated into the graphite in the reaction with $S_2O_6F_2$. First of all, although infrared spectra of the volatiles over the reaction mixture do show some $S_2O_5F_2$, this small amount can probably be attributed to the reaction of $S_2O_6F_2$ with the metal vacuum line and fittings in the reaction vessel. So the reaction probably does not involve the oxygenation reaction which is common for $S_2O_6F_2$:[9]

$$A + S_2O_6F_2 \longrightarrow AO + S_2O_5F_2.$$

Both the exothermicity of the reaction and the stability of the product towards pumping argue against any significant amount of neutral $S_2O_6F_2$ being incorporated. In other graphite compounds where neutrals are incorporated (e.g., SF_6 in $C_{12}GeF_6$)[14] or where neutrals are postulated to be in equilibrium with anions (AsF_3 and AsF_5 in C_8AsF_5),[4d,15] the neutrals are readily pumped off. Since $S_2O_6F_2$ is not polar enough for strong interactions with the graphite sheets or any anions present, and it is fairly volatile (140 torr at 25°C),[8] any neutral $S_2O_6F_2$ should pump out readily.

Heating C_xSO_3F yields sulfuryl fluoride. Comparison to the reaction:[16]

$$Ba(SO_3F)_2 \xrightarrow{350°C} BaSO_4 + SO_2F_2$$
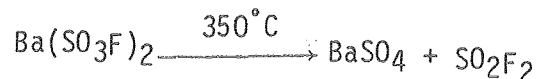
suggests that C_xSO_3F is in fact a simple ionic fluorosulfate. This

should be true for both the NASA graphite and HOPG products. The lower reactivity of HOPG is probably due to a higher activation energy required to initiate the formation of the first stage in HOPG samples. The formation of some first stage product in the room temperature reaction is probably influenced by two factors. Hooley[17] has shown that the thickness of an individual piece of graphite influences the threshold pressure of a reactant needed to initiate the formation of a given stage. So under the conditions employed here, the activity of the $S_2O_6F_2$ is probably sufficient to drive the more finely divided portion of the graphite to first stage. Local heating of the reaction should also raise the reactivity of the $S_2O_6F_2$, encouraging the formation of some first stage. In the case where nearly pure second stage HOPG fluorosulfate was produced, the slow introduction of $S_2O_6F_2$ minimized local heating, and only a small amount of first stage product was formed, despite the presence of a large excess of the peroxide.

2. <u>Second stage HOPG fluorosulfate.</u> The identification of this material as a second stage is firm. The c-spacing of 11.07 Å was determined from several reflections in the x-ray powder photograph, and this spacing is very nearly equal to the sum of a graphite layer (3.35 Å) and the thickness of a first stage (7.70 Å). And for second stage C_xSO_3F, $x > 13$, so the gallery filling is comparable to that found for the first stage material.

3. <u>Phase B.</u> The identity of phase B in the NASA graphite system is somewhat ambiguous. For graphite layer compounds of stage n, the strongest line in the powder pattern is expected to be the 00,n+1 (except in cases where the intensities are dominated by a very strong scatterer such as iridium). The only line attributable to the c-spacing in this phase has a d-spacing of 3.6 Å, suggesting c-spacings of either 7.2 Å for a first stage, 10.8 Å for a second stage, or 14.4 Å for a third stage. The stoichiometry is very nearly $C_{12}SO_3F$, so that the relative gallery fillings for each possibility correspond to occupied gallery stoichiometries of C_{12}, C_6, and C_4, respectively. This eliminates the third stage, since there simply is not sufficient space available for the fluorosulfates. The second stage C_6 (per occupied gallery) would require packing the fluorosulfates much more tightly than in the first stage, and the observed c-spacing is smaller than that found for the analogous HOPG compound (10.8 Å vs. 11.07 Å). However, the difference in charging between the NASA graphite product (C_{12}^+) and the HOPG product ($C_{x > 13}$) could account for some of the difference. A first stage formulation, with a $C_{12}SO_3F$ stoichiometry and a c-spacing of 7.2 Å could occur if the fluorosulfates in a layer tended to line up with vacancies in adjacent layers, as pictured in Figure 3-5. However, this would require a substantial distortion of the graphite lattice, which should be visible in the observed a-spacing.[18] The d-spacings attributable to 100 and 110 reflections are very close to those found for other graphite fluorosulfates, so this model can be ruled out.

4. <u>Acid fluorosulfates.</u> The reaction of C_xSO_3F with HSO_3F generally leads to a first stage compound with c-spacing larger than 7.7 Å, and the spacing appears to be a function of HSO_3F composition. Both the stability of these products toward pumping, and the observation that HSO_3F reacts with second stage materials to yield first stage, indicate that the incorporation of HSO_3F is very favorable. Hydrogen bonding to fluorosulfate anions within the gallery is probably the primary factor in the product stability. In addition, the neutral acid can serve as a dielectric material, screening the negative charges on the anions from each other. These effects are sufficiently favorable to open the unoccupied galleries of a second stage material to yield a first stage, even though there is no formal charge change.

The actual reaction that occurs when HSO_3F reacts with a first stage fluorosulfate is not clear. The c-spacing enlarges, so that the material appears to be similar to compounds made stoichiometrically from $S_2O_6F_2$ and HSO_3F. However, for the products to be the same would require displacement of SO_3F^- by HSO_3F to generate $S_2O_6F_2$. In attempts to observe $S_2O_6F_2$ generation from this system, none was observed. the The reactivity of $S_2O_6F_2$ in the presence of HSO_3F is very high, so that observing it might be difficult. In any case, it seems unlikely that HSO_3F should be capable of displacing such a stable anion as SO_3F^-, in spite of the lowered anion-anion repulsion this would produce.

There was generally a weight uptake associated with the reaction of first stage graphite fluorosulfate with fluorosulfonic acid, so the fluorosulfates in the acid product apparently is a bit more tightly

packed than in the acid free material. However, the considerable
scatter in the data made it impossible to determine how different
the stoichiometry limits of the two systems were. Other factors
which might contribute to the c-spacing variation will be discussed
in a subsequent section.

5. <u>Proton mobility in acid fluorosulfates.</u> For the NASA graphite
acid system, the HSO_3F in the galleries, or at least the H^+, must
be mobile to afford the ready homogenizing of the acid-free and acid
containing products. Since there should be a charge difference be-
tween $C_x(SO_3F,HSO_3F)$ (made stoichiometrically) and C_xSO_3F, there
should be a potential difference between the pair. Particles next to
each other in a mixture can be considered an electrochemical cell,
with overall reaction:

$$C_x^{1/x}SO_3F^- + C_x^{1/y}(SO_3F^-)_y(HSO_3F)_{1-y} \longrightarrow$$

$$2\ C_x^{(1/x\ +\ 1/y)/2}(SO_3F)^-_{(x+y)/2}(HSO_3F)_{(1-y)/2}$$
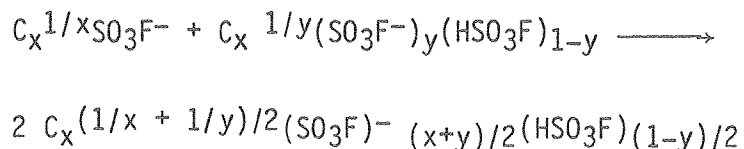
This reaction does not require the migration of any fluorosulfate. It
can be effected simply by H^+ transfer accompanied by electron trans-
fer through the conductive material.

The one attempt to reproduce this in the HOPG system gave a puzzling
result. The dominant set of c-spacings in the powder pattern indicated
a product that was much more like the parent acid containing material
than like an intermediate between the two parents. It should be noted
that the acid parent was not made stoichiometrically, so that, despite
its rather large c-spacing, its acid content might be very low. In

any case, whether this result for one measurement represents true differences of HOPG and NASA graphite, difference in the starting acid contents, or simply an experimental error could not be determined.

6. <u>Mechanisms for c-spacing variations.</u> The thickness of a carbon layer in α-graphite is 3.35 A. However, this represents the thickness of an uncharged sheet. Some contraction is expected as the layer becomes more positively charged, and this has been demonstrated for the system $C_{12}GeF_x$ ($5 \leqslant x < 6$),[14] where the c-spacing decreases as the charge increases, ranging from 8.2 Å to 7.8 Å, despite the increased bulk of the anion. This is also observed for C_9AsF_5 (c = 8.05 Å) compared to C_8AsF_6 (c = 7.85 Å).[4d] These represent unambiguous cases where the apparent thickness of the graphite decreases as a function of charge, and the magnitude of that change is similar to that observed for the fluorosulfate system. However, increased c-spacings were observed for the reaction of HSO_3F with first stage materials, where there should be not formal charge change without the unlikely displacement of $S_2O_6F_2$. So while this mechanism should be present, it must not be the only one operating here. Another consideration is the relative size of HSO_3F compared to SO_3F^-. The volume per formula unit in $K^+SO_3F^-$ is 92.5 Å^3.[19] The K^+, twelve coordinate in this structure, should have a radius of 1.60 Å,[20] and hence a volume of 17.2 Å^3. This leaves a volume of 75.3 Å^3 for the SO_3F. The density of pure HSO_3F is 1.7264 g/cc at 25°C,[21] a volume of 96.2 Å^3 per HSO_3F. However, the density of H_2SO_4 is 1.8267 g/cc,[21] giving a formula volume of 89.1 Å^3. Since these two acids are expected to be very similar

in size, and since the HSO_3F calculation suggests that the addition of a proton to SO_3F^- increases its volume by 21 $Å^3$, the density of HSO_3F must represent a non-close packed situation. 89 $Å^3$ is probably a better estimate of the true volume, and even this seems high, allowing 14 $Å^3$ for the volume of a proton.

If the volume change was accommodated entirely by increasing the c-spacing, a 7 $Å^3$ change (representing an equal mixture of HSO_3F and SO_3F^-) would require a roughly .35 $Å$ gallery height change. Again, the predicted change is of the correct size, but large c-spacings were observed for samples that probably do not have large acid content.

Another possibility to account for c-spacing changes involves structural changes. In the straight fluorosulfate, the anions would probably have to arrange themselves in such a way to minimize the c-spacing and thereby maximize the lattice energy. Hydrogen bonding when HSO_3F is present might encourage a different arrangement of the fluorosulfates in which hydrogen bridging between oxygen atoms on adjacent fluorosulfates is more favorable.

Four distinct arrangements for the fluorosulfates are shown in Figure 3-6. The average S-X bond distance in a fluorosulfate ion is assumed to be 1.46 $Å$, based on the bond distances found in KSO_3F[19] and NH_4SO_3F.[22] The Pauling van der Waals radius of X is taken as 1.39 $Å$, the weighted average for oxygen and fluorine.[23] Assuming that the thickness of a carbon layer is 3.35 $Å$, the predicted c-spacings are as indicated in the figure. All of the models give c-spacings that are too large to account for the c-spacings observed

in the first stage acid-free fluorosulfates. However, the calculations are for the thickness of a neutral carbon layer, and the reduction of that thickness due to charging should lower the c-spacings by a few tenths of an Angstrom. However, model A, at 8.51 Å, is much too large for this correction to be sufficient. Ruling out other possibilities is not straightforward. This problem led to attempts to obtain structural information from x-ray diffraction intensity measurements. The details of those studies (see Chapter 4) rule out models A and B, but the data was not sufficiently precise to choose between models C and D. The data does suggest that the arrangement could be a mixture of these latter models.

Of the three structures considered for explaining the variations in c-spacing, not one can be ruled out, nor is any one satisfactory. The expansion of first stage materials upon exposure to HSO_3F is probably due to the introduction of small amounts of acid into the gallery, without any formal charge change. The dielectric effect of the neutral species lowers the inter-anion repulsion so that the loss of lattice energy from expanding the c-axis is not prohibitive. In the cases where the first stage acid containing compounds were made stoichiometrically, the charge should definitely be lower than in the pure fluorosulfate. The observed c-spacings for these products show a monotonic increase as HSO_3F content increases. And treatment of an acid containing material with $S_2O_6F_2$ yielded a product of reduced c-spacing. These observations are consistent with a charging model. However, the average size of the guest species is also changing, and the potential influence of this should not be ignored.

7. Hydrogen abstraction and <u>in situ</u> HSO_3F generation reactions.
These reactions were judged on the basis of their quantitativeness.
Production of small quantities of SiF_4 was not considered a cause to
reject a reaction, since its generation is almost unavoidable when em-
ploying glassware with reactive fluorine compounds. For the abstrac-
tion reactions, H_2 was rejected because a large excess of H_2 was
required to show only a small c-spacing change; the HCl reaction, gen-
erating $S_2O_5F_2$, was not a clean reaction; and CHF_3 and PFTBA showed
no reactivity. Both <u>in situ</u> acid generation reactions showed side
products and were rejected.

8. <u>Differences in HOPG and NASA graphite systems.</u> For the most part,
the two graphites behaved similarly. The different reactivity towards
$S_2O_6F_2$ suggests that the activation energy for initiating a given
stage is larger for HOPG. Since HOPG is far more crystalline, this
could be influenced by a greater binding energy between the graphite
layers. In fact, the c-spacing for NASA graphite is larger than that
for HOPG, so it is less like α-graphite, the thermodynamically pre-
ferred modification. Other factors which could influence reactivity
include surface impurities (in spite of the heat treatment and fluori-
nation) and defects in the graphite.

The difference between phase B in the NASA graphite system and
second stage HOPG fluorosulfate is also a problem. A factor that
might be significant here is the long range ordering of the two graph-
ites, which will influence their abilities to direct a reactant to a
particular gallery, and thereby form a particular stage. HOPG shows

long range order, and the second stage material is well defined. The lack of long range ordering in NASA graphite might result in the formation of products with occupied galleries arranged randomly to one another, so that no distinct stage is formed until first stage. The d-spacing observed in the powder patterns would then be a weighted average of the graphite thickness and the occupied gallery thickness, and no other lines corresponding to a c-spacing should be observed. As more peroxide was introduced to the system, regimes of first stage material would be formed. While this is compatible with the general trends of the data, for the stoichiometry $C_{12}SO_3F$ a larger d-spacing is expected. The difference in the interaction of acid-containing and acid free products between the NASA graphite and HOPG systems is also not resolved, but may be influenced by the factors mentioned in that section.

9. _Summary_. $S_2O_6F_2$ reacts with graphite to produce intercalation compounds, and chemical and x-ray diffraction evidence is consistent with the incorporated species being the fluorosulfate anion. The first stage materials show stoichiometries C_xSO_3F, where $7.0 \leq x \leq 7.8$, and c-spacings between 7.6 Å and 7.7 Å.

Compounds of lower fluorosulfate content were also prepared. For HOPG, a second stage material with a c-spacing of 11.07 Å was observed. For the NASA graphite system, a phase with composition roughly $C_{12}SO_3F$ was observed, but this could not be structurally characterized.

Compounds which contained fluorosulfonic acid were synthesized, and these showed enlarged c-spacings, up to c = 8.04 Å. Factors potentially influencing the c-spacings included charging effects, changes in the guest species volume, and possibly reorientation of the guest species as a function of composition.

The protons of the acid containing material (at least for the NASA graphite system) were mobile, allowing samples of different acid content to equilibrate readily.

REFERENCES

1. A. K. Holliday, G. Hughes and S. M. Walker, Comprehensive Inorganic Chemistry, Vol. 1, p. 1250 ff. ed. Bailar et alia, Pergamon, Elsford, N.Y. (1973).

2. (a) G. R. Hennig, Prog. Inorg. Chem., 1, (1959) 125;

   (b) W. Rudorf, Adv. Inorg. Chem. Radiochem., 1 (1959) 223;

   (c) L. B. Ebert, Annu. Rev. Mater. Sci., 6 (1976) 181.

3. (a) Lin Chun-Hsu, H. Selig, M. Rabinowitz, I. Agranat and S. Sarig, Inorg. Nucl. Chem. Lett. 11 (1975) 601;

   (b) L. B. Ebert, and H. Selig, Mater. Sci. Eng., 31 (1977) 177;

   (c) G. Dresselhaus and M. S. Dresselhaus, Mater. Sci. Eng., 31 (1977) 235;

   (d) J. E. Fischer, J. C. S. Chem. Comm. (1978) 544.

4. (a) N. Bartlett, R. N. Biagioni, B. W. McQuillan, A. S. Robertson, and A. C. Thompson, J. C. S. Chem. Comm. (1978) 201;

   (b) N. Bartlett, B. McQuillan, and A. S. Robertson, Mat. Res. Bul., 13 (1978) 1259;

   (c) N. Bartlett, E. M. McCarron, and B. W. McQuillan, Synthetic Metals, 1 (1977/80) 221;

   (d) E. M. McCarron and N. Bartlett, J. C. S. Chem. Comm. (1980) 404.

5. M. J. Bottomley, G. S. Parry, A. R. Ubbelohde, and D. A. Young, J. Chem. Soc. (1963) 5674.

6. (a) G. Hennig, J. Chem. Phys. (1951), 922.

    (b) W. Rudorff and U. Hofmann, Zeit. Anorg. Allg. Chem., 238,
    (1938), 1;

    (c) S. Aronson, S. Lemont, and J. Weiner, Inorg. Chem., 10 (1971)
    1296.

7. D. Horn and H. P. Boehm, Mater. Sci., Eng., 31 (1977) 87.

8. F. B. Dudley and G. H. Cady, J. Am. Chem. Soc., 79 (1957) 513.

9. T. M. Shreeve and G. H. Cady, J. Am. Chem. Soc. 83 (1961) 4521.

10. (a) N. Bartlett and F. O. Sladky, J. C. S. Chem. Comm., 1968,
    1046;

    (b) M. Wechsberg, P. A. Bulliner, F. O. Sladky, R. Mews, and N.
    Bartlett, Inorg. Chem., 11 (1972) 3063.

11. A. M. Qureshi, L. E. Levchok, and F. Aubke, Can. J. Chem., 49
    (1971) 2544.

12. Stanley E. Livingstone, "Comprehensive Inorganic Chemistry," Vol.
    3, p. 1274, ed. Bailar, et alia, Pergamon, Elsford, N.Y. (1973).

13. R. L. Kirchmeier and J. M. Shreeve, Inorg. Chem., 12 (1973) 2886.

14. E. M. McCarron, Y. J. Grannec and Neil Bartlett, in print, Syn-
    thetic Metals.

15. E. R. Falardean, L. R. Hanlon, and T. E. Thompson, Inorg. Chem.,
    17 (1978) 301.

16. This is a synthetic approach to $S_2O_5F_2$: G. Braner, "Hand-
    book of Preparative Inorganic Chemistry," Academic, New York,
    1963.

17. J. G. Hooley, Mater. Sci. Eng., 31 (1977) 17.

18. As indicated in Figure 3-5, this formulation would require that at each vacancy, the carbon layer would pucker ˚4Å from a true planar arrangement. For an orderly array of fluorosulfates with $C_{12}SO_3F$ stoichiometry, the distance from vacancy to anion would be roughly 4.9 Å. If the carbon-carbon bond lengths remain the same as those of the known first stage material, the a-spacing would have to contract by a factor of cos[arcsin(.4/4.9)], or .33% with a corresponding .67% increase in the $1/d^2$ values. This size of increase would be very noticeable in the 110 reflection.

19. K. O'Sullivan, R. C. Thompson and J. Trotter, J. Chem. Soc. (A) (1967) 2024.

20. R. D. Shannon and C. T. Prewitt, Acta. Cryst., B26 (1970) 1076.

21. J. Barr, R. J. Gillespie, and R. C. Thompson, Inorg. Chem., 3 (1964) 1149.

22. K. O'Sullivan, R. C. Thompson and J. Trotter, J. Chem. Soc. (A) (1970) 1814.

23. L. Pauling, "The Nature of the Chemical Bond, 3rd ed. Cornell University Press, Ithaca, N.Y. (1960).

Table 3-1

	NASA GRAPHITE			HOPG		
	a = 2.458 Å			a = 2.461		
	c = 6.851 Å			c(α) = 6.709		
	c/2 = 3.425 Å			c(β)/2 = 10.063		
				c(α)/2 = c(β)/3 = 3.354		
hkℓ	I[a]	dobs	dobs	I[a]	hkℓ-α	(hkℓ-β)[b]
002	vs	3.426	3.359	vs	002	(003)
100	m	2.125	2.131	m	100	(100)
			2.084	w		(101)
			2.032	s	101	
			1.965	vw		(102)
			1.798	w	102	(103)
004	m	1.712	1.676	s	004	(006)
			1.541	m	103	
			1.318	vw	104	
110	m	1.229	1.229	ms	110	
			1.155	ms	112	
			1.134	vw	105	
			1.118	w	006	
			1.051	w	201	
			.993	m	114	

Table 3-1. (Continued)

NASA GRAPHITE		HOPG	
	.960	vw	203
	.838	w	008
	.827	mw	116
	.805	vw	210
	.799	mw	211

a) vs = very strong; ms = medium strong; s = strong
    m = medium; mw = medium weak; w = weak; vw = very weak

b) Many of the lines past the 009 – β can be indexed to a β phase.
    However, the weakness of the lines that are exclusively attribut-
    able to the β – phase suggest that the β – contribution should be
    insignificant.

Table 3-2. Reaction of C_xSO_3F with HSO_3F

Composition of starting material[a]	Product composition $C_x(SO_3F, HSO_3F)$		c-spacings in product, relative intensities[b]			a-spacing of product
	X Grav.	X, Anal.	Stage 1	Stage 2[c]	Graphite	
1	—	6.5	7.84 (vs)	—	—	2.450
1	—	7.3	7.85 (vs)	—	—	2.454
1 + B	6.0	6.8	7.77 (vs)	—	—	2.451
B		7.8	8.04 (vs)	—	—	2.454
1 + C	9.8	9.8	8.00 (s)	11.15 (m)	—	2.454
1 + C	—	—	8.1 (m)	11.2 (vs)	3.42 (m)	2.455
1 + C(tr)	—	7.5	7.98 (vs)	11.24 (vw)	—	2.453
1 + C(tr)	—	7.8	8.04 (vs)	—	—	—

a. 1 = 1st stage C_xSO_3F; B = phase B; C = graphite
b. Intensities listed are the powder pattern intensities for the given phase's dominant reflection.
c. Stage 2 values are based on the assumption that phase C is second stage.

Table 3-3. First stage $C_X(SO_3F,HSO_3F)$
produced stoichiometrically.

% SO_3F as HSO_3F	$(C_X(SO_3F,HSO_3F)$ Gravimetric X =	Analysis X =	Lattice C	Spacings a
58	6.1	6.6	7.80	2.449
59-61	6.7	——	7.87	2.448
				2.452*
69-72	7.6	7.6	7.95	2.449

*Duplicate run.

Table 3-4. Reaction of C_xSO_3F with hydrogen sources

Reactant	c-spacing of starting material	c-spacing of product	Species visible in the infrared spectra
$H_2(Pd)$	7.64	7.70	———
PFTBA	———	———	PFTBA, SiF_4
CHF_3	———	———	CHF_3, SiF_4
HCl	7.64	7.97	*$S_2O_5F_2$, SiF_4
HCl	7.70	7.96	———
HCl	———	———	*$S_2O_5F_2$, SiF_4

*For the experimental conditions, HCl would be difficult to detect.

Table 3-5. Products of HOPG + $S_2O_6F_2$

Reaction Conditions[a]	Product x(Grav.)	C_xSO_3F x(Anal.)	c-spacings, intensity,[b] Stage 1	Stage 2
$S_2O_6F_2$ l,RT	8.9	8.8	7.69 (w)	11.1 (s)
$S_2O_6F_2$ vap,RT	9.4	9.9	7.61 (m)	11.0 (s)
$S_2O_6F_2$ vap, 80°C	8.8	8.3	7.64 (vs)	11.0 (m)
$S_2O_6F_2$ excess in small volume	—	7.0	7.71 (vs)	—
Same	—	7.0	7.70 (vs)	—

a: l = liquid; vap = vapor; RT = ambient room temperature.
b: Intensities are powder pattern intensities of the dominant re-
   flection of a given phase.

Table 3-6. First stage HOPG fluorosulfate

a = 2.456
c = 7.727

hkℓ	calc	obs	Intensity
001	.0167	.0169	mw
002	.0669	.0675	vs
003	.1507	.1509	s
100	.2210	.2233	s
101	.2377	.2554	vw,br
004	.2679	.2881	w
005	.4186	.4188	vw
110	.6631	.6626	w
111	.6799	.6795	w
102	.7301	.7338	vw
113	.8138	.8114	vw
210	1.5473	1.5470	vw

Table 3-7. Second stage HOPG fluorosulfate with
first stage component

Second stage: c = 11.095
a = 2.456
First stage: c = 7.66

	Second state			First stage	
I	$1/d^2$obs.	$1/d^2$calc.	hkℓ	$1/d^2$calc.	hkℓ
w	.0171	.0081	001		
vw	.0167			.0171	001
w	.0328	.0324	002		
w	.0676			.0682	002
vs	.0737	.0724	003		
s	.1294	.1299	004		
w	.1528			.1535	003
s	.2214	.2210	100		
s,br	.2381			.2381	101
vw	.2580	.2535	102		
vw	.2747			.2730	004
m	.2934	.2924	006		
		.2942	103		

(Continued)

Table 3-7 (Continued)

I	Second stage			First stage	
	$1/d^2$obs.	$1/d^2$calc.	hkℓ	$1/d^2$calc.	hkℓ
vvw	.3811				
m	.3979	.3980	007		
s	.6613	.6631	110		
vw	.6978	.6956	112		
w	.7361	.7362	113		
vw	.7921	.7931	114		
vw	.8857	.8841	200		
vw	1.5461	1.5473	210		

Table 3-8. First stage HOPG acid fluorosulfate

$$a = 2.456$$
$$c = 8.013$$

I	$1/d^2$obs.	$1/d^2$calc.	hkℓ
w	.0156	.0155	001
vs	.0621	.0623	002
s	.1399	.1401	003
s	.2211	.2209	100
m	.2362	.2365	101
m	.2491	.2492	004
mw	.2827	.2832	102
vw	.3643	.3611	103
m	.3887	.3894	005
vw	.4686	.4702	104
m	.5603	.5607	006
w	.6637	.6629	110
w	.6795	.6785	111
vw	.7239	.7252	112
vw	.8848	.8839	200
vw	.8976	.8995	201
vw	.9976	.9968	008
w	1.5473	1.5468	210

$3.354 \, \overset{\circ}{A}$

$2.464 \, \overset{\circ}{A}$

α – graphite

(a)

$3.354 \, \overset{\circ}{A}$

$2.464 \, \overset{\circ}{A}$
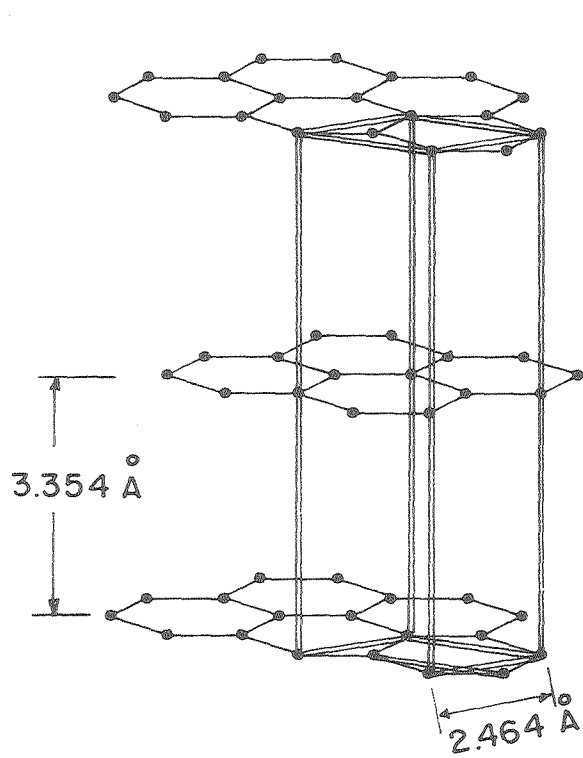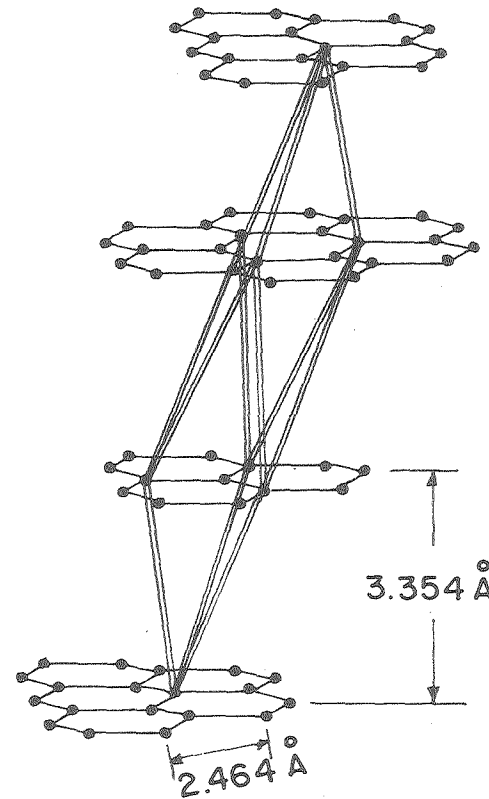
β- graphite

(b)

XBL 8010 – 6014

Figure 3-1. Structure of α- and β-graphite showing hexagonal (a) and rhombohedral (b) unit cells.

002
100
101β
101
102β
102
004
103
104
110
112
105
006
201
114
203
008
116
210
211

HOPG   NASA GRAPHITE
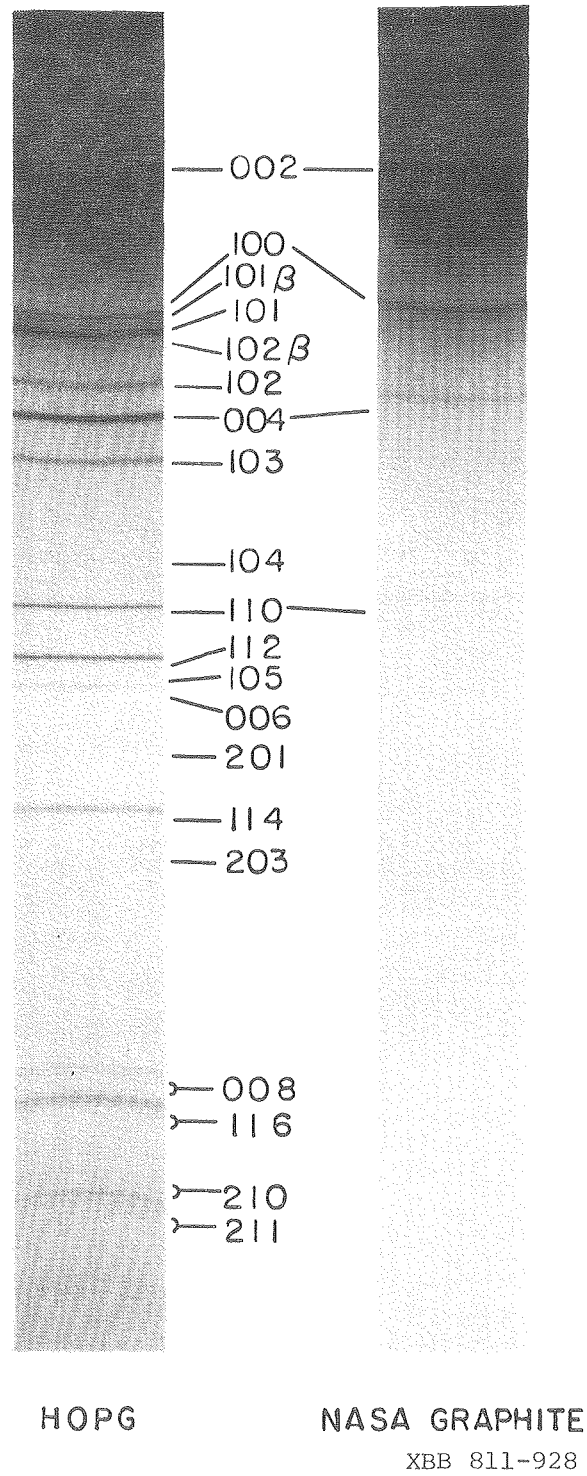
Figure 3-2. Powder patterns of graphites.

To
vacuum and $S_2O_6F_2$

Stainless steel
Whitey valve

Stainless
steel
union

Pyrex wool

To
HSO_3F
and vacuum

Kontes valve

Graphite sample
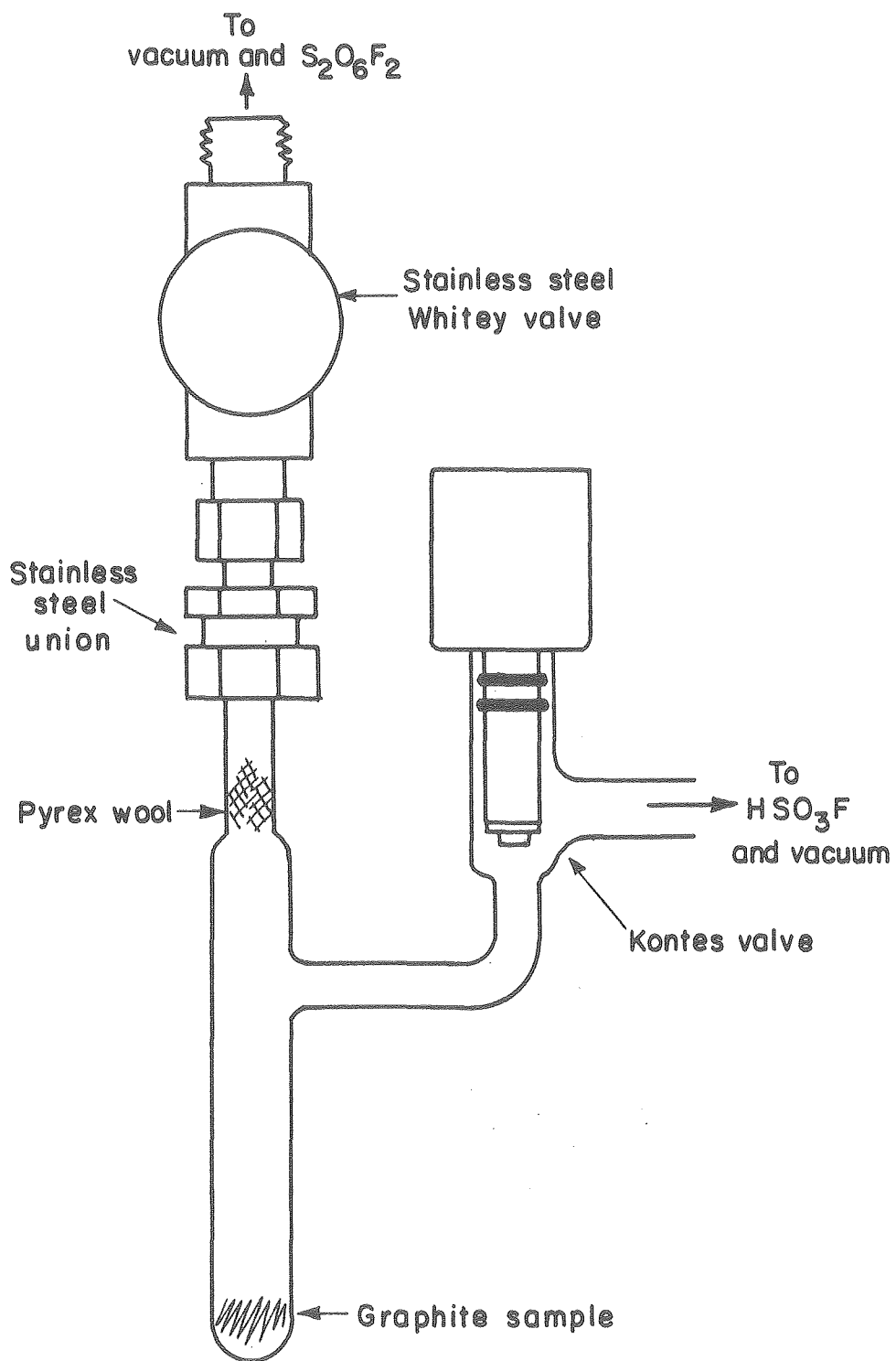
XBL8010-6007

Figure 3-3. Reactor for $C_x(SO_3F,HSO_3F)$ preparation.
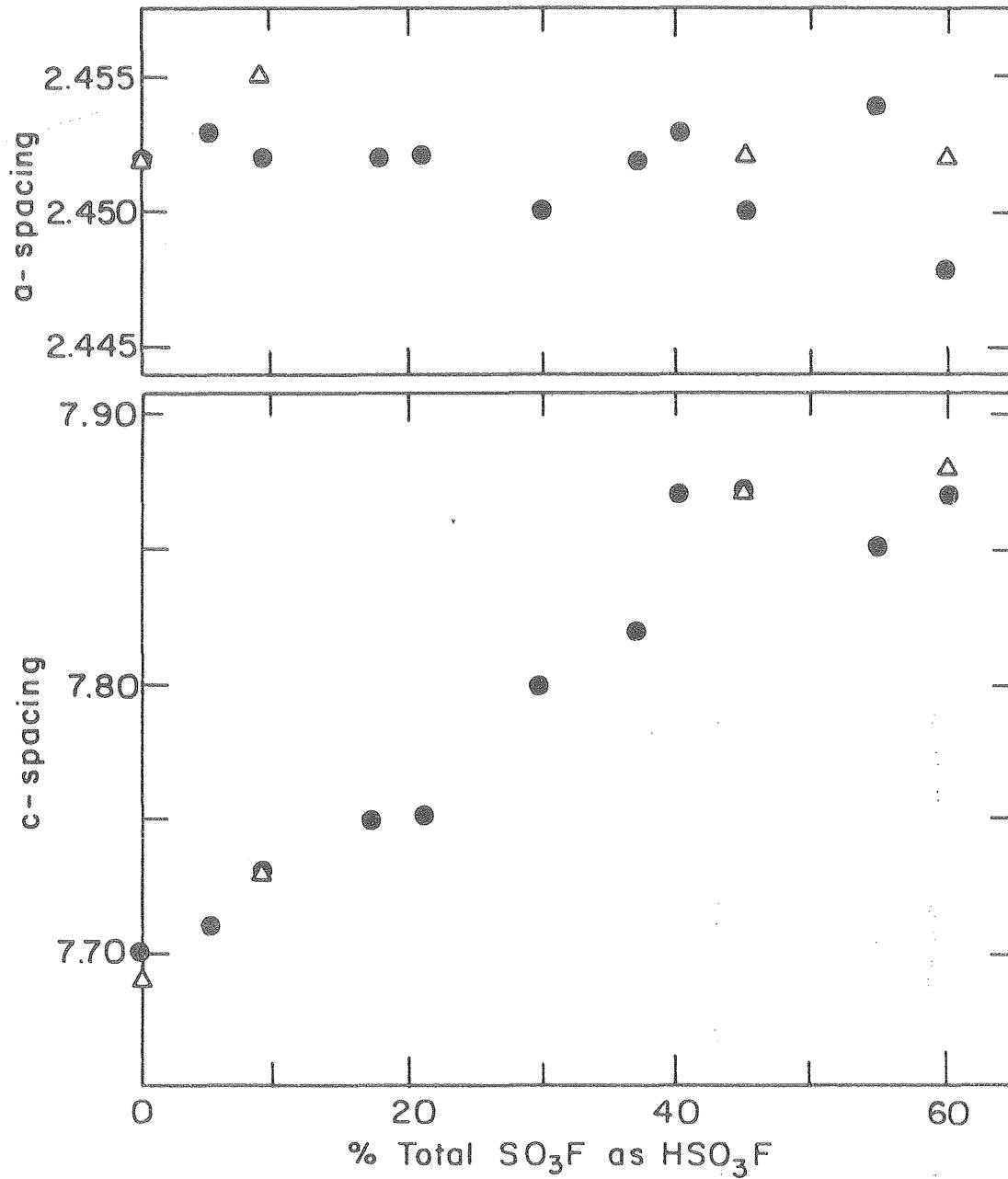
Figure 3-4. Lattice parameters vs. composition for $C_x(SO_3F,HSO_3F)$.
Triangles indicate duplicate run of a given composition.
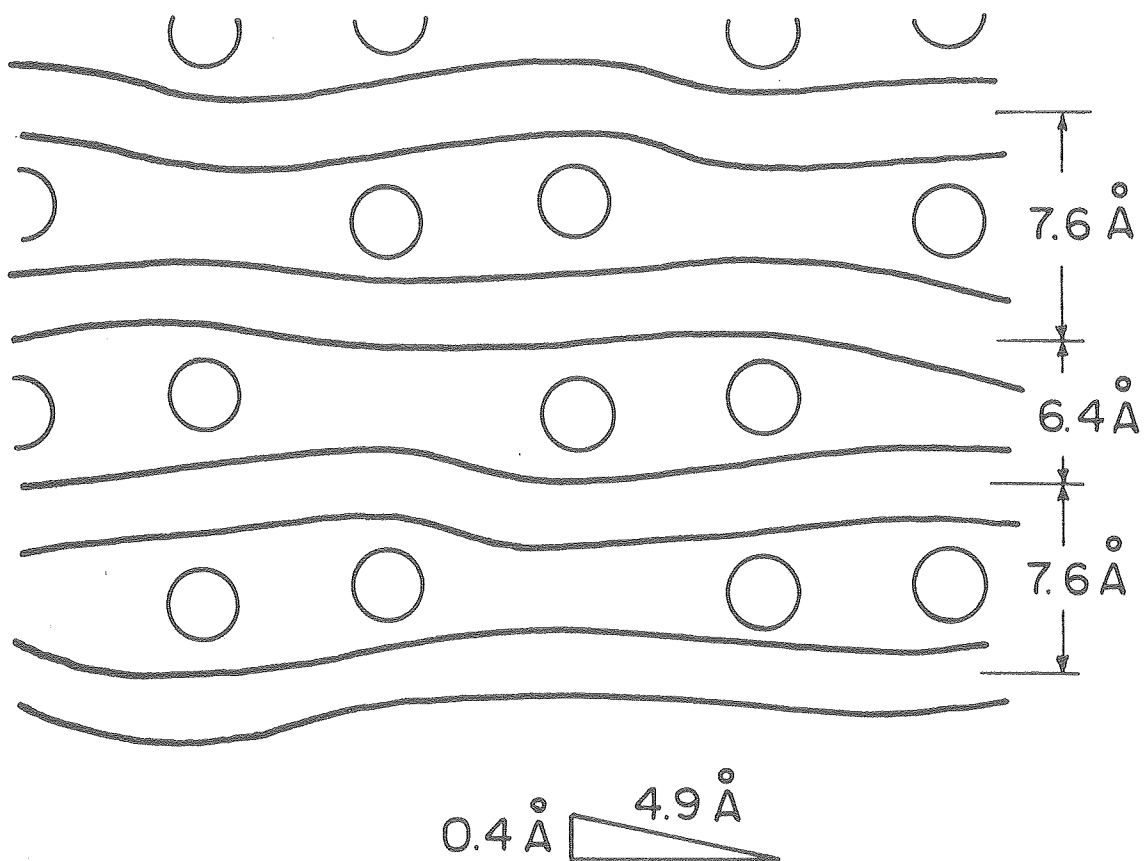
XBL 8010-6009A

XBL 8010-6010

Figure 3-5. Distortion that would be required for a first stage form-
ulation of phase B.
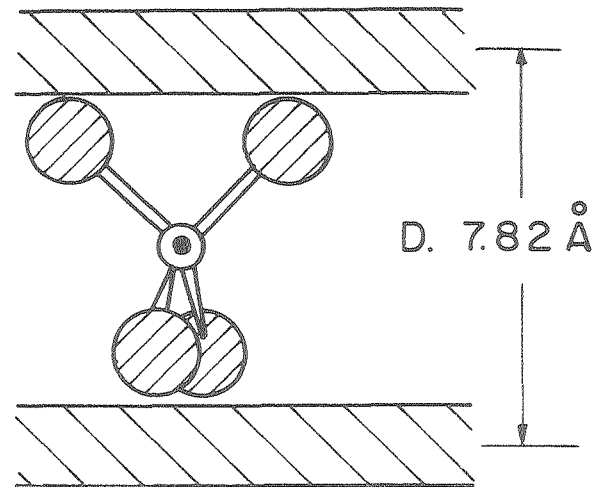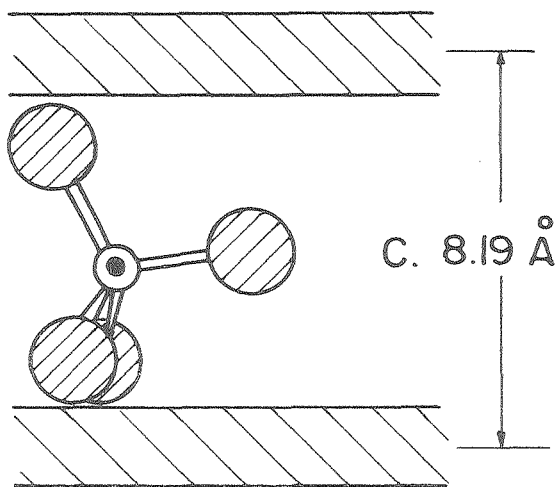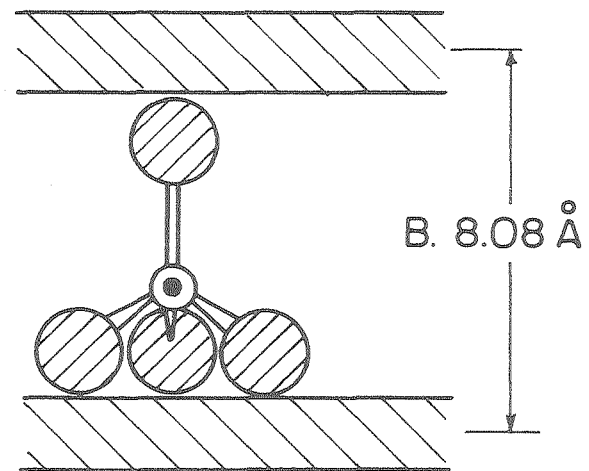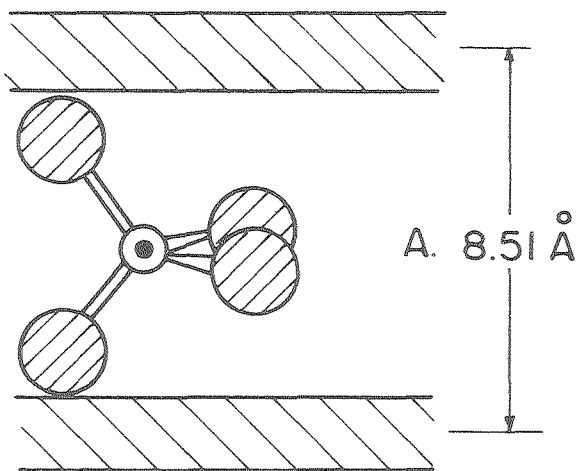
XBL8010-6011

Figure 3-6. Possible orientation for SO_3F and predicted c-spacings.

IV. STRUCTURAL CONSIDERATIONS IN GRAPHITE INTERCALATION COMPOUNDS

A. Introduction

1. Overview of some problems. While the chemical evidence mentioned
in the preceeding chapter indicated that C_xSO_3F was a simple ion-
ic structure, there was ambiguity regarding the possible effects of
structural changes in the HSO_3F containing material. Other work in
this laboratory dealt with conductivity studies on a variety of
graphite compounds. In these cases, chemical characterization was
based largely on gravimetric data coupled to the conductivity studies
and c-axis expansion measurements. However, there is debate among
various workers as to the nature of the species actually present in
the various systems, so some crystallographic studies were deemed
approximate.

At first consideration, a single crystal study would seem best.
Unfortunately, the natural single crystals that were readily available
were generally of very poor quality, usually twinned and showing
large c-axis spreads, as indicated in Figure 4-1. While good single
crystals could occasionally be found, previous experience in this lab
had shown that their integrity was often damaged in the intercalation
process.[1] Additionally, the stoichiometry of a reacted single
crystal could not be determined independently of the x-ray data.
Stoichiometry is influenced by a number of factors besides reaction
conditions. In particular, sample size affects the activity at which
formation of a given phase will be initiated.[2] The degree of crys-
tallinity of the graphite also influences reactivity, as demonstrated

by the differing behavior of NASA graphite and HOPG toward $S_2O_6F_2$.
In the same manner, the results obtained from HOPG studies do not ne-
cessarily apply to natural graphite studies.

Another problem, inherent in any study involving very small quan-
tities of materials, is insuring the chemical purity of the product in
situations where what would normally be regarded as trace impurities
are actually in significant quantity relative to the sample size. For
example, in an attempt to make a single crystal of C_8IrF_6, IrF_6
would be passed through a vacuum line that could contain some tungsten
residues (WF_6 is commonly used as a solvent in this laboratory). If
some WF_6 (which is more volatile than IrF_6) were formed, the sam-
ple composition could be seriously altered according to:

$$xC + IrF_6 + WF_6 \longrightarrow C_xWF_7 + IrF_5.$$

In a bulk sample preparation, this would be an insignificant problem,
but on a single crystal scale, it could lead to serious errors.

On the other hand, samples made from large pieces of HOPG would
avoid some of these problems. The stoichiometry of any given sample
could be defined fairly precisely, and the x-ray measurements could
potentially be made using the same sample used for a conductivity
study. Diffractometer tracings, originally only intended for c-spac-
ing determination, were already available for a large number of such
samples.

The purpose of this study was to ascertain the conditions for ob-
taining good x-ray intensity data, the limitations of the technique,
and then to try to analyze data to obtain structural information.

2. <u>Experimental approach and considerations.</u> For the experimental conditions employed here, only 00l data could be obtained. Complications which became apparent in the course of the work implied that portions of even these data were not reliable, so the size of the data set became even smaller. Rather than attempting a straightforward structural solution with these data, what was sought instead was a comparison of the observed intensity data with that calculated for various proposed models. To facilitate this, a computer program (listed in the appendix) was written to calculate structure factor sums, using a nine parameter fit for neutral atomic structure factors for C,O,F,P,S,Ge,As, and Ir, and also "O_3F" (average structure factor for three oxygens and one fluorine, as present in SO_3F).[3] The c-spacing (for $\sin\theta/\lambda$ determination) and the identity, multiplicity, z-parameter, and thermal factor for each unique atom were input for the desired model. The program allowed one parameter for one on the atoms to be varied in up to five steps between user specified limits, so that the effect of small changes in the model could be ascertained. For each variation in the model, the program calculated $F_{rel.}$, which was the predicted structure factor sum normalized to the sum of $|F|$ for 00l to 00,10. These numbers could then be compared to the similarly normalized $(I_{corr}/Lp)^{1/2} = |F_{obs.}|$, where the intensity was was adjusted for any defocusing effect, and Lp was the Lorentz polarization factor for the given geometry. The program also calculated powder pattern intensities [normalized to the 00(n+1) intensity for nth stage, with Lp corrections based on Cu $K\bar{\alpha}$ radiation)], so that powder data could be surveyed for structural information.

Some considerations led to the preference for Cu radiation rather than Mo radiation. First of all, for the type of geometry used here, i.e., narrow beam intercepted by a flat plate of thickness t, the absorption correction (actually a correction for effective scattering volume) is given by:[4]

$$\frac{1 - e^{-2\mu t/\sin\theta}}{2\mu}$$

when $\mu t/\sin\theta$ is sufficiently large, the term becomes a constant. Calculated values of μ for a number of species of interest to this lab are listed in Table 4-1.[5] These are based on an idealized C_8X composition, with c = 8.0Å. Conductivity measurement sample thicknesses typically were in the range of .05cm. It is clear that the absorption correction would be constant (and therefore unnecesssry) for the IrF_6 case, independent of choice of radiation. For GeF_6 and AsF_6, a small correction might be required at high angle if Mo radiation were used, but none should be needed for Cu or Cr radiation. For SO_3F and PF_6, no correction is needed for Cr radiation, and only a small correction for Cu radiation. But these samples are virtually transparent to Mo radiation, so not only would a large correction be needed, but the intensity of the beam passing through the sample would be great enough for scattering off the sample holder to be a problem.

Due to irregularities in the samples, it seemed preferable to choose a radiation that gave good depth penetration, so at first Mo radiation seemed to be the best choice for the germanium, arsenic and

iridium cases. However, for any given 001, the penetration depth τ is related to λ according to:

$$\tau \propto \frac{\sin\theta}{\mu} = \frac{1\lambda}{2\mu c} \quad .$$

Because λ for Kα Cu(1.5418 A) is about twice the size of λ for Kα Mo (.7107), while μ for Cu is also about twice the μ for Mo radiation, the overall effect is that the penetration depths for the two radiations are about the same. In contrast, despite λ being larger for Cr K$\bar{\alpha}$, the much larger μ makes the penetration depth much smaller. From these considerations, K$\bar{\alpha}$ Cu is the radiation of choice for the geometry employed in these studies.

B. Experimental

1. Sample preparation

    a. C_8IrF_6 diffractometer sample. Several HOPG samples, approximately 5mm square and of varying thicknesses, were heated to a red glow under vacuum and then treated briefly with fluorine. One of these, 45 mg, (3.75 mmoles C) was placed in a quartz tube-monel valve reactor. This was exposed to IrF_6, which was held in a monel can and cooled at $-78°C$ with a Dry-Ice acetone slush bath. As the slush bath warmed, the vapor pressure of the IrF_6 slowly increased so that the intercalation proceeded slowly. This was necessary to avoid gross distortion of the sample. After 10 hr., the excess IrF_6 vapor was condensed off. The weight uptake of 148 mg (.48 mmole) corresponded to the stoichiometry $C_{7.8}IrF_6$. The sample was a reflective blue, with a slightly rippled surface. It was cleaved to reveal a fresh surface

for the diffractometer study. The thickness of the freshly cleaved sample used for the study was ca. .4mm.

b. C_xIrF_6 powder. A sample of HOPG powder, 125 mg, (10.4 mmoles) was loaded into a quartz tube-monel valve reactor. Excess IrF_6 was condensed onto it, and allowed to react at room temperature. After the excess was condensed off, the weight uptake of 359 mg (1.17 mmole) corresponded to the composition $C_{8.9}IrF_6$. A sample of this was loaded into a .5mm quartz capillary, and an x-ray powder pattern obtained. The powder pattern showed a relatively strong pattern for a first stage (C = 8.01), with numerous other weak to very weak lines.

c. $C_x(SO_3F,HSO_3F)$ diffractometer sample. A pretreated 42mg HOPG sample (3.5 mmole) was loaded into a reactor of the type used for the $HSO_3F + C_xSO_3F$ studies. 26 mg HSO_3F (.26 mmole) was condensed onto this sample, and it was then exposed to $S_2O_6F_2$ held at $0°C$. Finally, a small amount of $S_2O_6F_2$ liquid was condensed onto the product and allowed to react for 30 minutes at $0°C$, and 30 minutes at room temperature. The excess S_2O_{6F2} was then pumped off. The weight uptake yielded an overall composition, $C_{7.4}(SO_3F,HSO_3F)$. If all the HSO_3F were consumed, the SO_3F content would be 55% HSO_3F. The sample had split into two pieces, and the outer surfaces were only moderately reflective. When fresh surfaces were exposed by cleaving, those fresh surfaces were more reflective, but did show some rippling. The sample used for the x-ray studies was .63mm thick.

d. C_xSO_3F diffractometer sample. Two pretreated graphite samples, 39 and 16mg, (3.25, 1.33 mmoles) were loaded into a reactor of the type used to make first stage HOPG fluorosulfate. The graphite

was exposed to $S_2O_6F_2$ held at $0°C$ for five hours, and then excess $S_2O_6F_2$ was condensed in. The reactor was then heated to $80°C$ for approximately one half hour. After the excess $S_2O_6F_2$ was pumped off, the larger chip showed a weight increase of 57mg ($C_{4.9}SO_3F$), and the smaller 23mg ($C_{5.6}SO_3F$). Both chips were partially cleaved in numerous places. The outer surfaces were very dull, and the edges very distorted. Interior surfaces did show some reflective portions, but the faces were not very flat. Due to the poor quality of these samples, no attempt was made to obtain intensity data.

2. Intensity data collection

a. Diffractometer tracings from conductivity studies. A large number of diffractometer tracings were available for samples that had been used for conductivity studies. However, in many cases, the more intense peaks were off-scale, so that their relative intensity could not be reliably determined. The tracings generally only extended to $2\theta = 80°$ (typically to 006), which was sufficient for c-spacing determination (the original purpose of these measurements) but which severely limited the size of the data set. Many of the tracings showed mixtures, so that the relative intensity could be seriously affected by the distribution of stages in the sample. The samples which were both single phase and on scale generally were not well defined stoichiometrically.

b. Diffractometer studies. A sample holder, shown in Figure 4-2, was fabricated. The sample could be mounted in the holder with a small amount of Halocarbor wax in the Dri Lab. A piece of .025mm thickness Kapton sheet was then placed over the holder, and a metal

ferrule pushed down over it, so that the Kapton was pressed against the o-rings. This Kapton dome provided protection from atmospheric moisture while the sample was handled outside of the Dri Lab.

Data were collected for the $C_{7.94}IrF_6$ sample and for the $C_{7.4}SO_3F$ sample. The sample handling was the same in each case.

Each sample was mounted on a goniometer and placed on a Nonius CAD-4 automated Diffractometer so that the primary beam, detector, and normal to the sample surface were all in the horizontal plane. A .5mm collimator was chosen to insure that the projection of the primary beam at low index would fall entirely on the sample. The sample was oriented visually first, and then intensity measurements with an upper and lower shutter were balanced by adjusting the goniometer arcs. The sample was rotated $90°$, and the procedure repeated. Sample height (relative to the goniometer) was adjusted to give consistent c-spacing values.

Intensity measurements were taken to $2\theta = 150°$ (to 00,10 for the iridium sample, to 009 for the fluorosulfate) using $\theta-2\theta$ scans, and a scan angle of $3°C$. Measurements were taken at $90°$ intervals around ϕ, the normal to the sample plane, such that the projection of the primary beam was along the sample diagonal. Background was subtracted from the raw data, and the Lorentz-polarization correction applied. The absorption correction for the Kapton dome was considered negligible relative to the scatter in the data. The thickness of the iridium sample was such that no relative absorption correction was needed. For the fluorosulfate sample, the small correction (approximate 7% in the most severe case) was applied. The normalized $|F_{obs.}|$ are listed are

listed in Tables 4-2 and 4-3. The c-spacing found for the iridium sample was 8.04 Å; for the fluorosulfate, 7.85 Å. The uncorrected I's, illustrating the pronounced variation of intensity as a function of ϕ, are listed in Tables 4-4 and 4-5.

For each sample, there were large variations in the observed intensities as a function of . After the data were collected, each sample was inspected under a microscope, but no unusual surface features were noted. In each case, the samples showed some loss of reflectivity in comparison with their appearance when freshly cleaved.

c. Powder pattern intensity measurement for $C_{7.5}(SO_3F,HSO_3F)$. While powder patterns of graphite compounds are quite adequate for determining unit cell dimensions, they are generally not of sufficient quality for intensity measurements. Most lines are fairly weak, and the background is usually strong. The powder pattern of $C_{7.5}(SO_3F,HSO_3F)$ made from powdered HOPG and listed in Table 3-8, was of exceptional quality for a graphite compound.

The intensity measurements were accomplished using a microdensitometer of the Dobson type described by Taylor.[6] Measurements were taken at .1mm intervals through the areas of interest, with measurements taken at larger intervals away from the peaks to determine background. The 003, 005, and 006 peaks were measured in this manner. The 004 line, though clearly resolved from the 100 to the eye, overlapped with that peak, which in turn overlapped with the 101 peak, so the entire region was measured and the 004 peak deconvoluted graphically. The 008 was visible to the eye, but the densitometer could not

detect it. The 002 peak was saturated, and the background around it strong, so it was not measured. The 007 was not visible on the film.

The intensity data were plotted out. Relative intensity was judged by photocopying the plot of each peak three times, and then cutting out and weighing the plotted peaks. Since some judgment was involved in deciding where a peak ended and background started, this method allowed one to cut out the peaks for differing possible back-grounds. The relative intensities of the 003, 004, 005 and 006 peaks are listed in Table 4-6. However, it should be noted that, to the eye, the 005 was more intense than the 004, which was more intense than the 006. So the measured intensities should be considered suspect.

C. Interpretation of Intensity Data

1. C_8IrF_6

a. Models for C_8IrF_6. If the species present in C_8IrF_6 is actually IrF_6^- as chemical evidence indicates, some predictions can be made. For an undistorted octahedral IrF_6^-, with Ir-F bond length estimated as ca. 1.85 Å,[7] and van der Waal's radius of 1.35 Å for fluorine,[*] the thick-ness of the IrF_6 entity along as threefold axis is predicted as 4.81 Å. With 3.35 Å added for a carbon layer, and with the IrF_6 oriented with a 3-fold parallel to c, the predicted c-spacing is then 8.16 Å, which is slightly larger than the observed 8.04 Å. The discrepancy can be attributed to contraction of the carbon layer thickness due to charg-ing. For a unit cell chosen with carbon at $z = 0$ (where the z parame-ter for each atom is its fractional position along the c-axis), and the iridium at $z = .500$, the fluorine atoms should be at $z = .367$. This will be referred to as the octahedral model".

If, on the other hand, the IrF_6 unit does not remain intact, the iridium might not be located at z = .500. The fluorine position should still be near z = .367, since this value is primarily determined by the van der Waal's radius of a fluorine and the thickness of a carbon sheet. This will be referred to as the "fluorination model," since this type of arrangement could occur if the IrF_6 fluorinated the graphite and formed some less symmetrical Ir species.

b. Comparison of models to diffractometer data for C_8IrF_6. Table 4-7 lists the following: The average values of $|F_{obs.}|$; the values of $|F_{calc.}|$ calculated for the octahedral model; with a thermal parameter B = 4 4^2 chosen arbitrarily; the predicted powder pattern intensities for that model; and the observed relative intensities for the first stage 00 lines of the powder pattern. It is immediately apparent that the data for the 001 and 002 peaks do not correspond at all to the predicted F_{rel}. Moderate variation in the fluorine parameter (from z = .350 to .375) does not improve the agreement. The fluorination model shows the same problem. However, in the powder data, the 001 line is relatively strong. Both models predict that the 001 should be stronger than the 002 in the powder pattern. However, the use of a relatively large capillary (.7mm) for the x-ray powder measurement introduces a substantial obsorption problem, causing a progressively more severe loss of intensity towards lower angles. So the observed intensity of the 001 is expected to be significantly less than predicted. From this evidence, it appears that the problem is more in the low angle diffractometer data than in the choice of models. The error is probably induced by irregularities in the sample surface. This should be particularly

crucial in the Ir sample, where sample penetration by the x-ray beam is very small, especially at low angles. Another factor which could be influential is the possibility of a thin surface impurity. As mentioned earlier, the samples showed a loss of reflectivity after the data set was taken. Because of the high absorption coefficient, a very thin surface coating of deteriorated sample could introduce a serious change in relative intensity, especially at low angle where the effective pathlength through a surface layer is very large. A 3 micron impurity on the surface would cause the observed intensity of the 001 to drop by a factor of one half relative to the 002.

The anticipated problems should generally be less severe at higher angles, so an attempt was made to evaluate the models using higher angle data only. Since the observed intensities of the low angle reflections were assumed to be lower than they should be, it was necessary to renormalize the $F_{obs.}$ so that the sum of these for the 004 to 00,10 reflections was adjusted to match the average sum for the corresponding $|F_{calc.}|$ for each model. Table 4-8 lists the renormalized $(F_{obs.})$ for the octahedral model, along with the relative $F_{calc.}$ for a range of fluorine parameters. Table 4-9 lists the corresponding information for the fluorination model.

While agreement between calculated and observed F's is never particularly good, it is apparent that the octahedral model is generally much better than the fluorination model. In particular, when the Ir is moved away from $z = .500$ in the fluorination model, the relative intensity of even numbered reflections to adjacent odd numbered reflections changes dramatically from the general tendency in the data

for odd-numbered reflections to be weaker than nearby even-numbered reflections. In contrast, while the octahedral model does not give particularly good numerical agreement, it does predict the stronger-weaker variation seen in the data. For this reason, the octahedral model was considered to be the correct model, although small displacement of the iridium from $z = .500$ cannot be ruled out.

Due to the scatter in the data, it did not seem justifiable to try to optimize the fit past this point.

2. $C_{7.4}(SO_3F, HSO_3F)$

a. Structural models for $C_x(SO_3F, HSO_3F)$. Table 4-10 illustrates the various idealized orientations for fluorosulfate in graphite that were mentioned in Chapter III. The oxygen and fluorine atoms will be considered equivalent, and will be referred to simply as "X". In general, the carbon-X distance will be determined primarily by the carbon thickness and X van der Waal's radius, with an allowance for some contraction of the carbon layer due to charging. For a starting point, the X position can be taken as $z = .375$, and experience with this type of calculation has shown that small variations in its z parameter will not greatly change the relative $F_{cal.}$ for the models chosen. Each model should predict a distinct set of $F_{calc.}$ dependent on two major factors: the relative number of X at .375 and near .500; and displacement of sulfur from $z = .500$. For the various models, idealized starting parameters are listed in Table 4-10. The carbon parameter is taken as $z = 0$. While a small out of plane distortion cannot be ruled out, the constancy of the observed a-spacings for a wide range of c-values (see in particular Figure 3-3), and the similarity of the a-spacings

to that of graphite argue against any major distortion of the carbon lattice.

b. Comparison of models to diffractometer data for $C_x(SO_3F,HSO_3F)$. The data for $C_{7.4}(SO_3F,HSO_3F)$ showed large variation in intensity as a function of ϕ (see Table 4-5), so it was apparent that irregularities in the sample were significant. Preliminary comparison of the data to the $F_{calc.}$ for the various models showed that the same problem observed in the C_8IrF_6 data set, abnormally weak low angle reflections, was also present here, alhtough the problem was not as severe. Again, the data was renormalized to the 004 to 009 of the $F_{calc.}$ for each model.

Table 4-11 lists the $|F_{calc.}|$ and normalized $|F_{obs.}|$ for each model. Model A predicts that the 003 and 005 will be much weaker than the 004 and 006, contrary to the trend in the data. Model B predicts that the 004 and 006 will be weak relative to the 003 and 005, again contrary to the data. Both of these models were rechecked for a range of parameters, but no satisfactory fit was found. While models C and D did not give good numerical fits, they at least predicted F's of the right magnitudes, so they were used as the basis of further calculations. The effect of varying atomic positions for each of the two models and for combinations of them was checked. The best fit for a relatively simple model corresponded to an equal mixture of C and D, with the sulfur position for model C moved to $z = .44$. The fit is listed in Table 4-12. Perhaps fortuitously, if the position of a sulfur atom for model C is calculated from the S-X bond length (rather than from its position relative to X arbitrarily placed at $z = .375$) the predicted position is at $z = .44$.

This fit is not meant to be a definitive statement of structure by any means. Rather, it is suggestive that some of the sulfur (but not all of it) is out of the $z = .500$ plane, while some of the X is away from $z = .375$. Whether or not the presence of some X in the $z = .500$ plane is related to the possibility of hydrogen bonding cannot be determined. A good set of data for a well defined series of varying HSO_3F content would be needed to test the effect of acid on the structure.

c. Analysis of powder pattern intensities. The intensity data from the powder pattern of $C_{7.5}(SO_3F,HSO_3F)$ with c-spacing $c = 8.04$ Å, was similarly compared to predicted powder pattern intensities for the various models. The choice of parameters that gave the best fit was again an equal mixture of models C and D, but with the sulfur of model D at $z = .47$. The comparison of predicted intensities to normalized observed intensities is shown in Table 4-13. However, if the relative intensities as judged visually are correct, the fit is erroneous. The visually judged relative intensities correspond to model D. Due to this uncertainty, no conclusions should be drawn from this particular study.

To test the technique, a few lines from a moderately weak powder pattern of potassium fluoride were measured. The observed and calculated intensities for the measured reflections are listed in Table 4-14. The fit is only fair in this case, where the powder pattern lines were relatively sharp against a clean background. Overall, the quality of the graphite fluorosulfate powder pattern was poorer, with weaker, more diffuse lines against a stronger background. In this case, near the limit of the densitometer's sensitivity, any dust or

scratches on the film would seriously effect the measured intensities. So the reliability of the graphite fluorosulfate powder pattern measurement was very low.

d. Further structural aspects of the graphite fluorosulfate system. Unlike many other graphite systems, the fluorosulfate system does not tend towards stoichiometries that are consistent with registry with the carbon network. For first stage materials, the composition of $C_x(SO_3F,HSO_3F)$ generally has $7.0 \leqslant x \leqslant 7.8$. No extra lines were ever observed in the powder patterns corresponding to a true unit cell dimension in the graphite plane. However, in the HOPG samples, general hkl reflections are present, so there is apparently sufficient local ordering for the carbon sheets to register relative to one another in both the first and second stage compounds.

The stoichiometry can be rationalized on the basis of nonclose packed arrangements of the fluorosulfates. In a first stage compound with c = 7.7Å, allowing 3.35Å for the carbon layer, the gallery volume available per carbon in 11.3 $Å^3$, so for a 75 $Å^3$ SO_3F, the close packed stoichiometry would be $C_{6.6}$.

However, if the gallery height is not restricted, allowing the fluorosulfates to closepack as shown in Figure 4-3a results in 11.6 $Å^2$ being required for each fluorosulfate. At 2.6 $Å^2$ per carbon, this corresponds to a $C_{4.5}$ stoichiometry. But this arrangement, corresponding to model B (Table 4-10) requires a much larger c-spacing than that found for first stage acid free fluorosulfates. The orientation that seems most probable for small c-spacing structures is that of model D (Table 4-10) (although there is admittedly no independent evi-

dence for this), since it requires the least gallery height. The closest packing for this orientation is shown in Figure 4-3b, where the in plane packing of the X atoms is essentially square. For this arrangement, the predicted stoichiometry is $C_{5.2}$. This arrangement, however, would not allow any rotational freedom. But the powder patterns of small c-spacing materials always show a very quick drop off in 001 intensity, suggesting that there is a good deal of thermal motion contributing to a large thermal factor. Allowing each anion sufficient room to rotate freely around the c-axis, as shown in Figure 4-3c, predicts a $C_{8.9}$ stoichiometry, so totally free rotation is apparently not possible. However, the slower drop off of 001 intensity in the acid containing materials could well be a consequence of hydrogen bonding hindering rotational motion.

The factor which probably is most influential against close packing in the acid free system is anion-anion repulsion. For a close packed system with stoichiometry $C_{4.5}$ and a c-spacing near 8 Å, each anion would be surrounded by six anions at 4.06 Å, nearly as close as the carbon sheet, so the lattice energy would certainly be positive. This problem, along with the increasing work function of the graphite network, is probably more influential in limiting composition than any volume considerations.

3. Conclusions. The x-ray intensity data sets for $C_{7.8}IrF_6$ and $C_{7.4}(SO_3F, HSO_3F)$ are consistent with relatively simple structural models.

For $C_{7.8}IrF_6$, the iridium atoms must lie near the $z = .5$ plane, with the fluorine atoms near $z = .37$. This fits an octahedral IrF_6^-, with a threefold axis parallel to c.

The data for $C_{7.4}(SO_3F,HSO_3F)$ could not be fit to any one of the four presented models. However, two of the models could be ruled out, and a combination of the other two models provided a qualitative fit. This fit suggested that some of the oxygen atom occupancy was at $z = .5$, and that the sulfur atoms were not all at $z = .5$.

For both the iridium hexafluoride and fluorosulfate samples, the data sets showed too much scatter for any precise fit to be attempted.

REFERENCES

1. E. M. McCarron, and T. Mallouk, unpublished results.

2. J. G. Hooley, Mat. Sci. Eng. 31 (1977) 17.

3. International Tables for X-ray Crystallography, Vol. 4, p. 99, Kynoch, Birmingham, Eng. (1974).

4. Ibid, Vol. 2, p. 291 (1965).

5. Ibid, Vol. 3, p. 162 ff. (1965).

6. A. Taylor, J. Sci. Instr. (1951) 250.

7. Estimated to be similar to the Ir(VI)-F distance in IrF_6, M. Kimura, U. Schomaker, D. W. Smith, and B. Weinstock, J. Chem. Phys., 48 (1968) 4001.

8. L. Pauling"The Nature of the Chemical Bond," 3rd ed., Cornell University Press, Ithaca, N.Y., (1960).

Table 4-1. $\mu(cm^{-1})$ for C_8X.

X	Cr 2.2909	λ Cu 1.5418	Mo .7107
SO_3F	74	19.4	2.7
PF_6	86	27	3.0
GeF_6	145	46	29
AsF_6	158	51	33
IrF_6	614	233	127

Table 4-2. C_8IrF_6 $|F_{obs..}|$

l	$\phi = -30°$	$60°$	$150°$	$-120°$	Ave
1	20	88	18	75	50
2	252	267	207	301	256
3	28	21	20	23	23
4	228	172	201	172	193
5	75	57	74	56	66
6	225	172	214	166	194
7	87	57	81	68	73
8	131	98	113	101	111
9	35	24	28	24	28
10	50	33	41	37	40

Table 4-3. $|F_{obs.}|$ $C_{7.4}(SO_3F, HSO_3F)$.

	$\phi = -30°$	$60°$	$150°$	$-120°$	Ave
$l = 1$	12	12	13	12	12
2	254	263	291	271	270
3	168	180	177	173	175
4	108	115	101	108	108
5	142	140	128	139	137
6	120	111	108	117	114
7	54	48	50	52	51
8	98	88	89	94	92
9	45	40	41	43	42

Table 4-4. Uncorrected intensity data for C_8IrF_6.

1	$\phi = -30°$	$60°$	$150°$	$-120°$
1	15625	328	5957	355
2	16,135	44,368	16,378	51,516
3	122	192	106	187
4	5521	7880	6620	7163
5	436	628	600	541
6	2857	4211	3976	3506
7	351	496	472	368
8	826	1176	980	89
9	81	104	89	72
10	380	425	392	391

Table 4-5. Uncorrected intensity data for $C_{7.4}(SO_3F, HSO_3F)$.

l	$\phi = -30°$	60°	150°	-120°
1	1737	2947	2101	1847
2	379,395	617,874	490,872	435,914
3	102,015	175,982	111,586	108,658
4	28506	48699	24571	28362
5	34649	51120	27876	33179
6	18216	23684	14494	17392
7	3124	3732	2374	2819
8	10977	13408	9034	10223
9	3526	4165	3018	3238

Table 4-6. Powder pattern intensities for $C_{7.5}(SO_3F, HSO_3F)$, $c = 8.04$

hk ℓ	I (arbitrary units)
003	300
004	50
005	36
006	11
007	unobserved
008	observed, not measurable

Table 4-7. Comparison of octahedral model for C_8IrF_6 to
diffractometer and powder data.

1	$\lvert F_{obs.}\rvert$	$\lvert F_{calc.}\rvert$	$I_{calc.}$	$I_{obs.}$
1	50	193	1803	m
2	256	291	1000	s
3	23	8	0	vw
4	193	117	35	w
5	66	47	3	
6	194	130	16	—
7	73	74	3	—
8	111	82	4	—
9	28	29	1	—
10	40	29	1	—

Table 4-8. C_8IrF_6 (octahedral model). $F_{calc.}$ compared to $|F_{obs.}|$, varying fluorine position.

	$|F_{obs.}|$	Z = .355	.360	.365	.370	.375
1	*	-184	-188	-191	-194	-197
2	*	271	281	288	295	302
3	18	5	0	-5	-11	-17
4	151	126	122	118	116	114
5	52	-68	-59	-50	-42	-33
6	151	147	141	133	125	118
7	57	-77	-77	-76	-72	-68
8	87	76	80	82	83	84
9	22	-21	-25	-28	-31	-34
10	31	25	26	28	30	32

For carbon at Z = 0; Ir at Z = .500

*001,002 discarded.

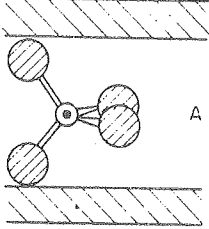Table 4-10.

MODEL A

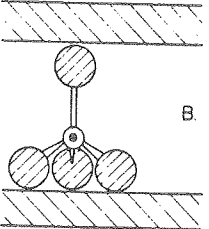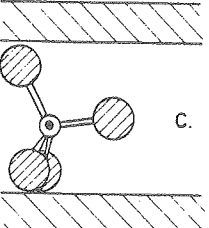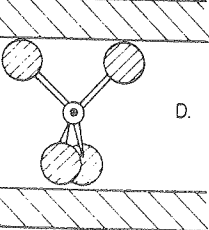   S $Z = .500$

    2X $Z = .500$

    2X $Z = .375$

MODEL B

    S $Z = .44$

    4X $Z = .375$

MODEL C

    S $Z = .47$

    3X $Z = .375$

    X $Z = .500$

MODEL D

    S $Z = .500$

    4X $Z = .375$

Table 4-11. Comparison of $|F_{obs.}|$ to $|F_{calc.}|$
for various models of $C_x(SO_3F, HSO_3F)$.

A	$|F_{calc.}|$	$|F_{obs.}|$	B	$|F_{calc.}|$	$|F_{obs.}|$
1	2	—	1	36	—
2	383	—	2	293	—
3	75	155	3	250	129
4	175	96	4	14	80
5	33	121	5	176	101
6	141	101	6	50	84
7	15	45	7	55	38
8	109	81	8	61	68
9	7	37	9	42	31

C	$|F_{calc.}|$	$|F_{obs.}|$	D	$|F_{calc.}|$	$|F_{obs.}|$
1	17	—	1	20	—
2	351	—	2	306	—
3	158	141	3	202	133
4	112	88	4	67	82
5	90	112	5	109	104
6	113	93	6	113	87
7	11	42	7	8	39
8	90	75	8	112	70
9	22	34	9	3	32

Table 4-12. "Best fit" for $C_{7.4}SO_3F_1HSO_3F$ diffractometer data.

$$
\begin{array}{lll}
8 & C & Z = 0 \\
3.5 & X & Z = .375 \\
.5 & X & Z = .500 \\
.5 & S & Z = .500 \\
.5 & S & Z = .440
\end{array}
$$

	$\lvert F_{obs.}\rvert$	$\lvert F_{calc.}\rvert$
3	135	199
4	83	71
5	105	120
5	88	95
7	39	18
8	71	88
9	32	20

Table 4-13. Fitting powder pattern intensity data for
$C_{7.5}(SO_3F, HSO_3F)$.

$$7.5 \ C \quad Z = .000$$
$$3.5 \ X \quad Z = .375$$
$$.5 \ X \quad Z = .500$$
$$.5 \ S \quad Z = .500$$
$$.5 \ S \quad Z = .470$$

	$I_{calc.}$	$I_{obs.}$
3	130	127
4	18	21
5	13	15
6	9	5
7	0	0
8	5	W

Table 4-14. Powder pattern intensities for KF.

hkl	$I_{calc.}$*	$I_{obs.}$*	$I_{vis.}$**
311	159	169	4
200	310	234	2
400	115	181	3
331	65	87	5
420	352	330	1

*Normalized to $\Sigma I = 1000$

**Visually estimated relative intensities, with "1" greatest.
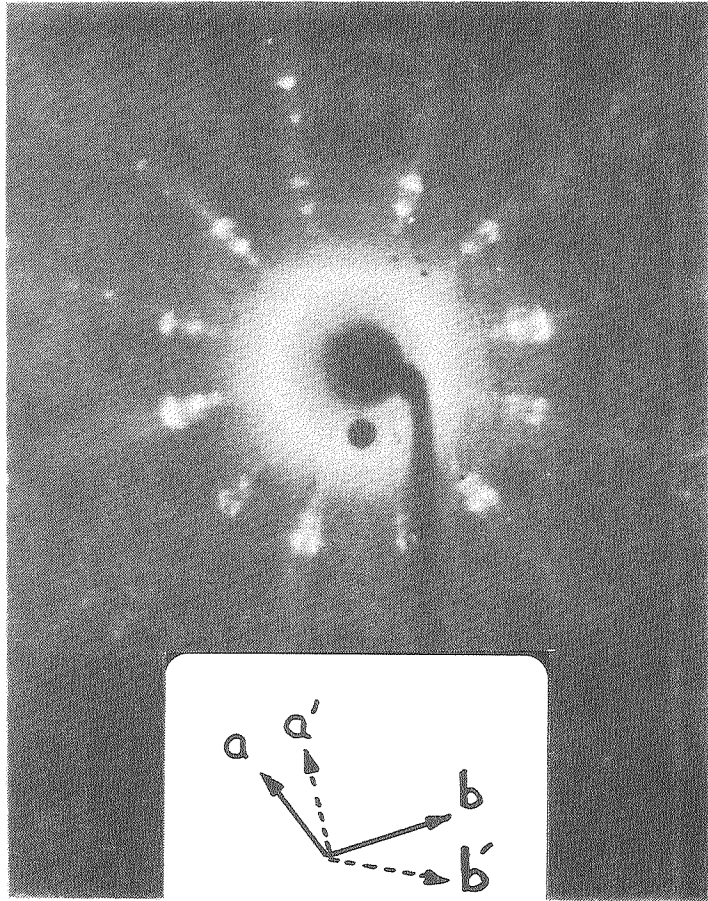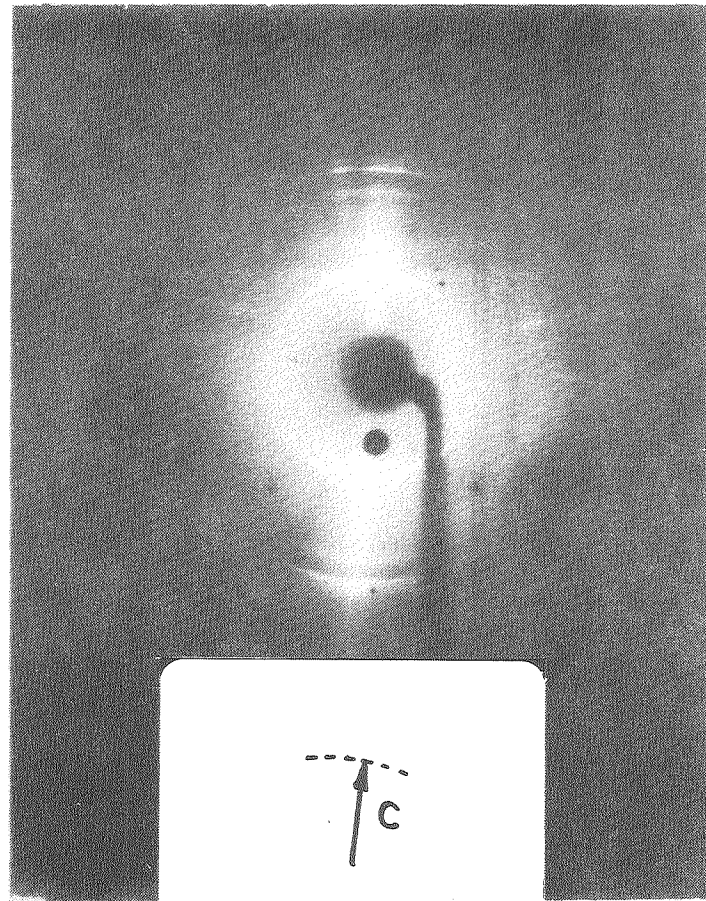
XBB 800-11426A

Figure 4-1. Typical precession photographs of graphite crystals, un-
filtered Mo radiation, showing a) twinning and b) c-axis spread.

(a)

(b)

(c)

XBL 8010-6008

Figure 4-2. Holder for HOPG diffractometer samples, a) overall view, b) with Kapton covering and ferrule in place, c) positioning of sample.

(a)

2.38Å + 2.78Å = 5.16Å

Tetrahedron base

Tetrahedron apex

(b)

5.16 Å

Tetrahedron viewed along 2-fold axis

(c)

5.54 Å

Tetrahedron allowed rotation motion around 2-fold axis

XBL 8010-6012

Figure 4-3. Close packing models for graphite fluorosulfates.

V. BORON NITRIDE FLUOROSULFATE
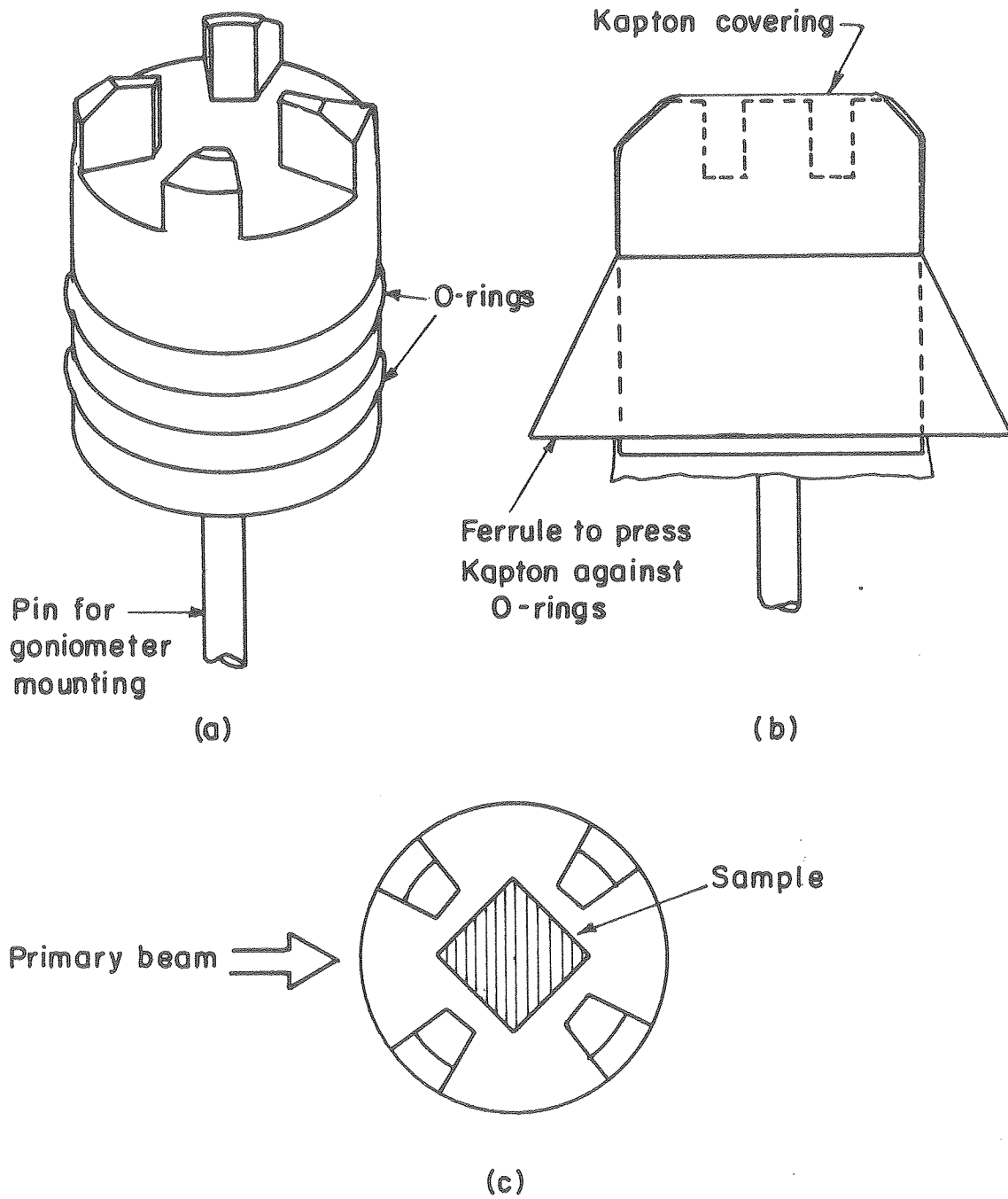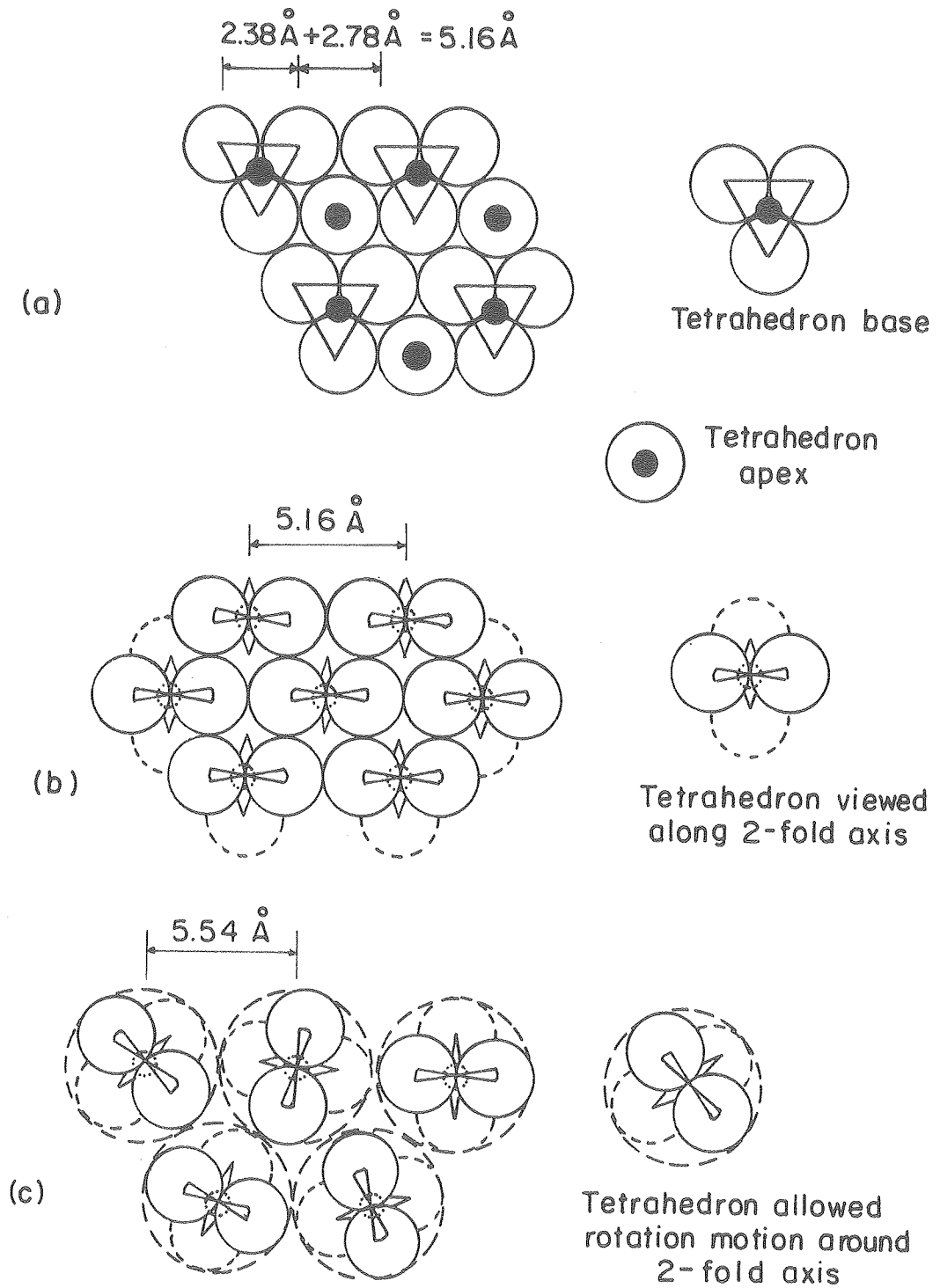
A. Introduction

A boron-nitrogen unit is isoelectronic with a carbon-carbon unit, so comparative studies of carbon systems and their boron-nitrogen analogs are of interest. The hexagonal layered form of boron nitride is appropriate to this study as an analog of graphite. The structural similarities[1] indicated in Figure 5-1 are immediately evident, with the relative stacking of the planes being the only noteworthy difference. On the other hand, boron nitride differs from graphite in many properties.[2] Graphite, dark gray in color, is a semimetal. In contrast, boron nitride is colorless, and an excellent insulator. The lack of conductivity in boron nitride is generally ascribed to a band gap between the filled pi (valence) band and empty pi* (conduction) bands,[3] as shown in Figure 5-2.

Boron-nitrogen compounds exhibit quantitative differences from their carbon analogs. Although borazine ($B_3N_3N_6$) formally analogous to benzene and like it a planar molecule, the electron delocalization in borazine is less extensive, i.e., both of the canonical forms shown in Figure 5-3 are important.[4] For the extended boron nitrogen system in born nitride, B^{11} n.m.r. studies have indicated that there is significant delocalization.[5] Although the crystal structure allows for some deviation from planarity, the deviation must be small.[1]

Up to the time this work was started, there were no reliable reports of boron nitride intercalation. Croft[6] reacted boron nitride with a variety of reagents, and observed weight uptake in many cases.

When heated rapidly, his products exfoliated,[7] so Croft maintained that his products were intercalation compounds. However, Rudorff and Stumpp[8] were not able to reproduce Croft's results, and they noted that Croft described his starting material as "glossy black," whereas pure boron nitride is colorless. Other claims for uptake of guest species have been reported,[9] but the products have been characterized neither chemically nor structurally. In any case, there were no previous claims for a first stage compound.

The powerful oxidizers available in this laboratory suggested a possibility of producing boron nitride intercalation compounds. However, the greater lability of boron nitride compared with graphite did limit the choice of oxidizers. In particular, both fluorine and hydrofluoric acid destroy boron nitride, as reported by Glemser and Haeseler[10]:

$$BN + HF \longrightarrow NH_4^+ BF_4^-$$

$$BN + F_2 \longrightarrow N_2 + BF_3 \; .$$
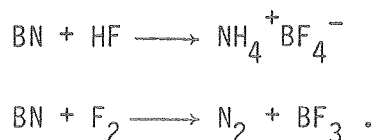
Graphite does not react with either HF or F_2 at ambient temperature.

B. Starting materials and reactants

1. Powdered boron nitride. This was obtained from Ventron, (Beverly, Mass.) and was used for the bulk of this work. This material was very finely powdered, and also well ordered, as judged from powder patterns. This material was dried in ca. 100°C oven. The technique used for drying graphite powder, i.e., flaming under vacuum was generally not employed. The very finely powdered BN tended to get

ₔucked into the valve during this type of heating process.

2. <u>Highly ordered boron nitride (HOBN)</u>. A few small pieces of boron nitride, analogous to HOPG, were obtained from Union Carbide, courtesy of Dr. Arthur Moore. This material was translucent with a slightly brown tint.

3. $S_2O_6F_2$. Prepared as described in Chapter III.

4. HSO_3F. Distilled into small Pyrex ampules.

C. <u>Experimental</u>

1. <u>Reaction of powdered boron nitride with $S_2O_6F_2$</u>. Powdered borron nitride was loaded into a preweighed reaction vessel of the type used for preparing graphite fluorosulfates. $S_2O_6F_2$ was condensed in excess over the powder and allowed to react at room temperature. On some occasions, the bottom of the vessel was immersed in an ultrasonic cleaning device to help break up unreacted clumps and to facilitate mixing. Slight effervescence was occasionally noticeable. The color change from white boron nitride to blue-black product was usually complete within one-half hour. In one instance, the vapors over the reaction mixture was examined by infrared spectroscopy. Only $S_2O_6F_2$ was observed, but the presence of a small amount of $S_2O_5F_2$ cannot be ruled out, since its bands largely overlap those of $S_2O_6F_2$. Excess $S_2O_6F_2$ was then pumped off, and the resultant stoichiometry determined by weight change. Stoichiometries determined in this manner varied from $(BN)_{2.2}SO_3F$ to $(BN)_8SO_3F$. The final product varied in appearance from a wet, dark material, through a blue-black, free-flowing powder, to a light blue powder.

2. <u>Routine x-ray powder photography</u>. Powder patterns of the reacted boron nitride, loaded into capillaries in the Dri Lab, always showed some unreacted boron nitride, and frequently the pattern due to the unreacted material was dominant. The product contained in capillaries often showed signs of decomposition before the x-ray exposure could be completed, based on the loss of sample coloration.

3. <u>Samples prepared capillaries</u>. To circumvent the need to handle the product in the Dri Lab, boron nitride was reacted with $S_2O_6F_5$ in capillaries. Powdered boron nitride was loaded into capillaries each joined to valve via a FEP tube heat-sealed to the capillary, as shown in Figure 5-4. The reactor assembly was previously passivated with $S_2O_6F_2$. $S_2O_6F_2$ was condensed onto the boron nitride and allowed to react. Temperature cycling between room temperature and $-196°C$ helped to mix the reactants and expel bubbles which occasionally formed. Excess $S_2O_6F_2$ was then pumped off very slowly. Three outcomes were typical. Often, the expanding boron nitride would block the capillary, preventing the $S_2O_6F_2$ from reaching part of the sample. Other times, attempts to remove excess $S_2O_6F_2$ resulted in the formation of bubbles which ejected the product from the capillary. And the extensive handling involved in temperature cycling frequently resulted in capillary breakage.

In one instance, a sample of boron nitride was reacted in a 1.0mm capillary to yield a homogeneous blue-black product. The capillary was mounted on the Debye-Scherrer camera and cooled to $-80°C$ using the low temperature device. A malfunction of the low temperature device prevented the sample from being kept cold for the entire exposure, so

the resultant powder pattern is representative of the product at both room temperature and low temperature. Despite the breakdown, the powder pattern so obtained showed no trace of unreacted boron nitride, so all the observed reflections could be attributed to product. A listing of the powder pattern is given in Table 5-1.

4. Stability. The stability of boron nitride fluorosulfate was quite variable. Prolonged pumping on a powdered sample at room temperature usually resulted in a weight loss and diminished coloration. However, a few samples showed stability towards pumping. However, even the best samples, stored in dry quartz ampules, showed degradation within a few weeks.

When a tube containing several-day-old boron nitride fluorosulfate was opened to an infrared cell, the spectrum showed only BF_3 and $S_2O_5F_2$, and no sign of $S_2O_6F_2$.

5. Reaction of powdered boron nitride with $S_2O_6F_2$ in fluorosulfonic acid. In a nitrogen filled glove box, excess HSO_3F was poured onto a sample of powdered boron nitride held in a quartz reaction vessel. No reaction was evident. A valve was attached to the reaction vessel, the mixture cooled to $0°C$, and the nitrogen pumped off. Excess $S_2O_6F_2$ was then condensed onto the mixture and allowed to react at room temperature. Within approximately one half hour, the boron nitride darkened to a deep blue product. However, the attempt to pump off the excess volative reactants lead to product decoloration.

In one attempt to repeat the experiment, the boron nitride did not appear to react with the $S_2O_6F_2$, judging by the lack of color change.

No further attempts to prepare or characterize these materials were made.

6. Reaction of HOBN with $S_2O_6F_2$. Highly ordered boron nitride was re-
acted with $S_2O_6F_2$ on two occasions. In the first case, a single piece
of boron nitride (27.2mg, 1.10 mmole) was reacted with $S_2O_6F_2$. No reac-
tion was apparent after thirty minutes at room temperature, and the sam-
ple showed only slight discoloration after one hour at 70°C. The reac-
tion was allowed to procede overnight at 70°C. This resulted in a prod-
uct that was homogeneously dark colored, opaque, and split into several
pieces. The chips appeared slightly blue by reflection. There were al-
so some droplets of a non-volatile material present. The chips were
weighed in a separate container in the Dri Lab. The weight uptake (29.7
mg, .30 mmole SO_3F) corresponded to the stoichiometry $(BN)_{3.7}SO_3F$.

In another instance, $S_2O_6F_2$ was reacted with HOBN (26.5 mg, 1.07
mmole) which had been broken into small pieces. At room temperature,
some effervescence was evident. After two hours at room temperature,
the chips were obviously darkened. The reaction proceded at room tem-
perature overnight, yielding a dark blue product. The weight uptake
after excess $S_2O_6F_2$ was removed (20.2mg, .20mmole SO_3F) indicated
the stoichiometry $(BN)_{5.5}SO_3F$.

7. X-ray precession photography. Chips of reacted HOBN were mounted
in quartz capillaries, using a small amount of pyrex wool to hold the
samples in place. In some cases, the chips were treated with $S_2O_6F_2$
again in situ. In each case, precession photographs showed a strong
set of reflections corresponding to unreacted boron nitride 001 re-
flections, and a weak set of reflections along the same axis corre-

sponding to a spacing of 8.05 Å. Despite careful handling, these materials always degraded within a few hours.

8. <u>Conductivity measurements.</u> Pieces from the HOBN flurosulfate preparations were tested crudely for conductivity using a battery operated volt-ohm meter. Typically, a sample of a few millimeters across showed a resistance of about 3000 ohms.

D. <u>Discussion</u>

1. <u>Composition.</u> The presence of only $S_2O_6F_2$ in the infrared of the vapors over the reaction mixture is consistent with the SO_3F unit remaining intact. No BF_3 generation was observed during the reaction. Although some effervescence was noted during the reaction, it was not sufficient to represent a product of the main reaction, and could have been a result of incomplete drying of the starting material.

The observation of $S_2O_5F_2$ as an ultimate decomposition product is also consistent with the presence of fluorosulfate, according to the reaction:

$$A(SO_3F)_2 \longrightarrow A = 0 + S_2O_5F_2.$$

Since the incorporated unit is SO_3F, and there was no major loss of either boron or nitrogen during the course of the reaction, the formulation of the product as "$(BN)_xSO_3F$" is meaningful.

The value of x determined gravimetrically varied widely. This is the result of a number of factors. First, it was impossible to reliably remove all of the excess $S_2O_6F_2$ without also decomposing the product. The instability of the product, as evidenced by both its generation of $S_2O_5F_2$ and BF_3, and by its discoloration, also made reliable gravimetry difficult. However, the observed stoichiometries did

suggest the idealized stoichiometry $(BN)_4SO_3F$, similar to the roughly $C_{7.5}SO_3F$ stoichiometry found for the graphite analog.

2. <u>Structural information</u>. The combination of powder data and precession data indicate that this is in fact a layer compound based on a boron nitride framework. The precession data showed that the c-axis of the product was parallel to that of the parent boron nitride. The powder data listed in Table 5-1 shows two major features. First of all, there are reflections corresponding to the 100, 110, and 210 reflections of boron nitride, while the absence of the very strong boron nitride 002 reflection indicates that the parent material is not present. The a-spacing determined from these reflections is a = 2.502 Å, essentially the same as for boron nitride, a = 504 Å.[1] This indicates that the boron nitride layers are intact, and that any induced non-planarity, if any at all, must be very small. The powder data also shows a set of 001 reflections similar to those observed for the HOPG acid fluorosulfate. In particular, the 008 relfection is visible, while the 007 is not. This relative intensity is predicted for each of the structural models considered for graphite fluorosulfate in the preceding chapter. However, the overall quality of the x-ray powder photograph prevented any relative intensity measurement for the 002 through 006 reflections, which would be required to establish the fluorosulfate orientation.

The c-axis spacing (powder data, c = 7.99 Å; precession data, c = 8.05 Å) is considerably larger than that found for the corresponding graphite fluorosulfate (c = 7.7 Å), but similar to that found for some of the acid fluorosulfates. The larger c-spacing could be a re-

sult of fluorosulfate orientation. In an oxidized boron nitride, the boron should bear more of the positive charge than the more electronegative nitrogen. This would encourage the anions to orient to increase the boron coordination number. Orientation of SO_3F with its three-fold axis parallel to $\underline{c}$ is acceptable with this situation.

The rather large uncertainty in the stoichiometry also allows the possibility that the boron nitride galleries are filled more tightly than their graphite counterparts, which could also produce an enlarged c-spacing.

3. <u>Ionic character of boron fluorosulfate</u>. The conductivity of boron nitride fluorosulfate is consistent with the removal of electrons from the filled valence band. The deep blue color of this material, reminiscent of the color observed for graphite intercalation compounds, is also consistent with a partially oxidized delocalized system. Strongly covalent interaction between the BN layers and SO_3F would require that the BN be non-planar, but any large non-planarity can be ruled out from the x-ray data. These observations suggest that boron nitride fluorosulfate should be considered as the salt $(BN)_x^+ SO_3F^-$.

4. <u>Comparison of boron nitride fluorosulfate with graphite fluorosulfate</u>. Overall, the two systems appear more similar than different. Both appear to be predominantly ionic structures, with anions packed between essentially planar parent networks. The overall stoichiometries are analogous.

The reactivity of HOBN chips suggests that the intercalation mechanism is similar to that occurring in the graphite system. Smaller pieces of HOBN reacted more readily than did larger pieces. For the

graphite system, Hooley[10] has shown that the thickness of a graphite chip influences the reagent activity required to initiate the formation of a given stage, and that this is related to the influence of mechanical stresses involved in opening galleries. At least for the very limited set of observations available here, this is also applicable to the boron nitride system.

No evidence of stages other than first stage was ever observed for the boron nitride system. This could be a result of the lack of conductivity in the parent boron nitride. In graphite, the inherent conductivity allows a given intercalated layer to influence the electronic structure of nearby layers, so that the attacking species is preferentially directed towards a given layer. In boron nitride, the ability of an intercalated layer to influence the electronic structure of a non adjacent layer should be much lower, so that the initiation point for the next attack should be more random. In this case, the only well defined product phase would be first stage.

Due to the difficulties encountered with the $BN/HSO_3F/S_2O_6F_2$ system, a study comparable to that made with the graphite system was not attempted. However, it should be noted that, at least in one case, an intercalation compound was apparently produced and it was stable in the presence of HSO_3F. So syntheses of materials $(BN)_x(SO_3F/HSO_3F)$ might in fact be feasible.

5. <u>Summary</u>. Boron nitride reacts with $S_2O_6F_2$ to produce a blue-black first stage intercalation compound, analogous to graphite fluorosulfate. The product is an electrical conductor, consistent with removal of electrons from the valence band of the boron nitride network. The structure

is ionic, with the boron nitride sheets planar. The product is chemi-
cally much less stable than its graphite analog.

REFERENCES

1. R. S. Pease, Acta. Cryst., 5 (1952) 236.

2. N. N. Greenwood and B. S. Thompson, Comprehensive Inorganic Chemistry, p. 916ff. ed. Bailar, et alia., Pergamon Press, Elmsford, N.Y. (1973).

3. R. Taylor and C. A. Coulson, Proc. Phys. Soc. A., 65 (1952) 834.

4. K. Niedzu and J. W. Dawson, Boron-Nitrogen Compounds, Springer-Verlag, Berlin, Heidelberg (1965).

5. A. H. Silver and P. J. Bray, J. Chem., Phys., 32 (1960) 288.

6. R. C. Croft, Austral. J. Chem., 9 (1956) 206.

7. Exfoliation is the rapid separation of the layers of a layer compound. It commonly occurs when graphite intercalation compounds are heated rapidly.

8. W. Rudorff and E. Stumpp, Z. Naturforsch., 13b (1958) 459.

9. (a) A. G. Freeman and J. P. Larkindale, Inorg. Nucl. Chem. Lett., 5 (1969) 937;

   (b) A. G. Freeman and J. P. Lackindale, J. Chem. Soc.(A) (1969) 1307.

10. O. Glemser and H. Haeseler, Z. Anorg. Allg. Chem., 279 (1959) 141.

11. J. G. Hooley, Mat. Sci. Eng., 31 (1977) 17.

Table 5-1. $(VN)_xSO_3F$.

$A = 2.502$ Å
$c = 1.993$ Å

hkl	yd^2(calc.)	yd^2(obs.)	I
001	—	.0427	vw
002	.0626	.0624	vs
003	.1408	.1403	s
100	.2129	.2157	s
004	.2504	.2483	s
	—	.3087	m
005	.3913	.3915	w
	—	.5185	w
	—	.5307	w
006	.5635	.5592	w
110	.6388	.6382	m
111	.6532	.6532	m
112	.7014	.6998	mw
113	.7797	.7792	w
200	.8518	.8505	w
	—	.8877	w
008	1.0019	1.0052	vw
210	1.4881*	1.4903	w
	—	1.5224	vw

*$K\alpha_1$.

3.354 Å   2.464Å

Graphite

3.330Å   2.504Å
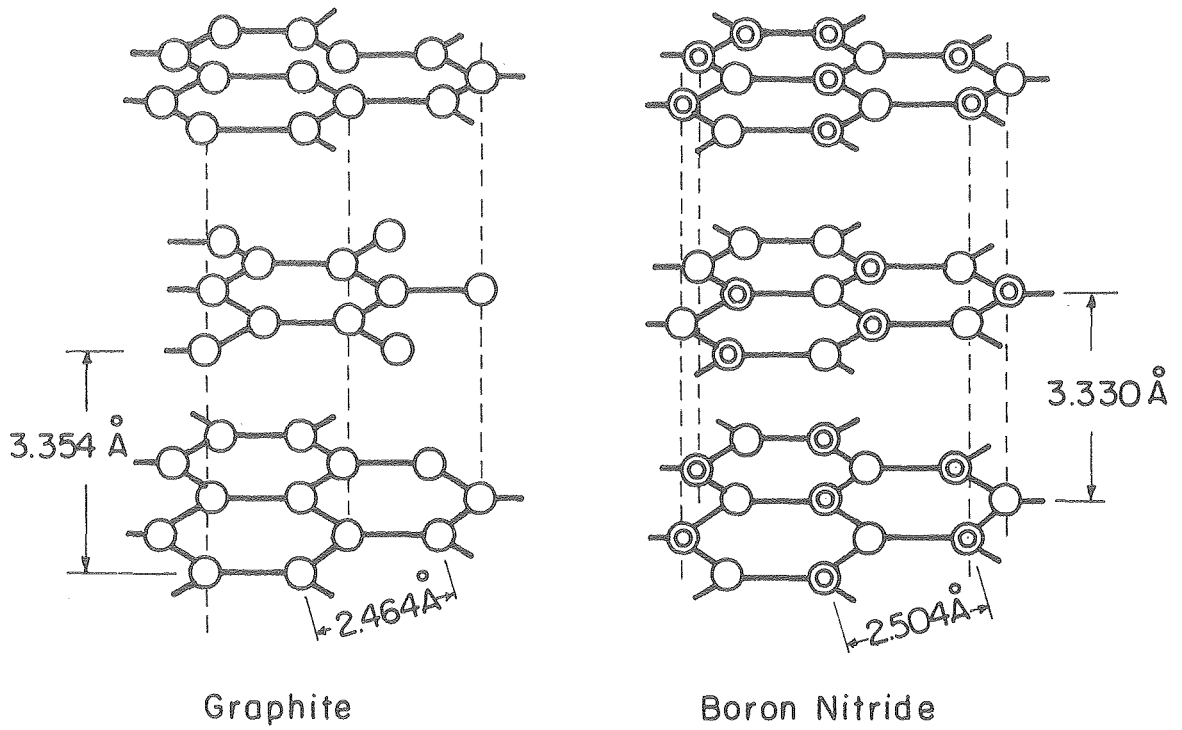
Boron Nitride
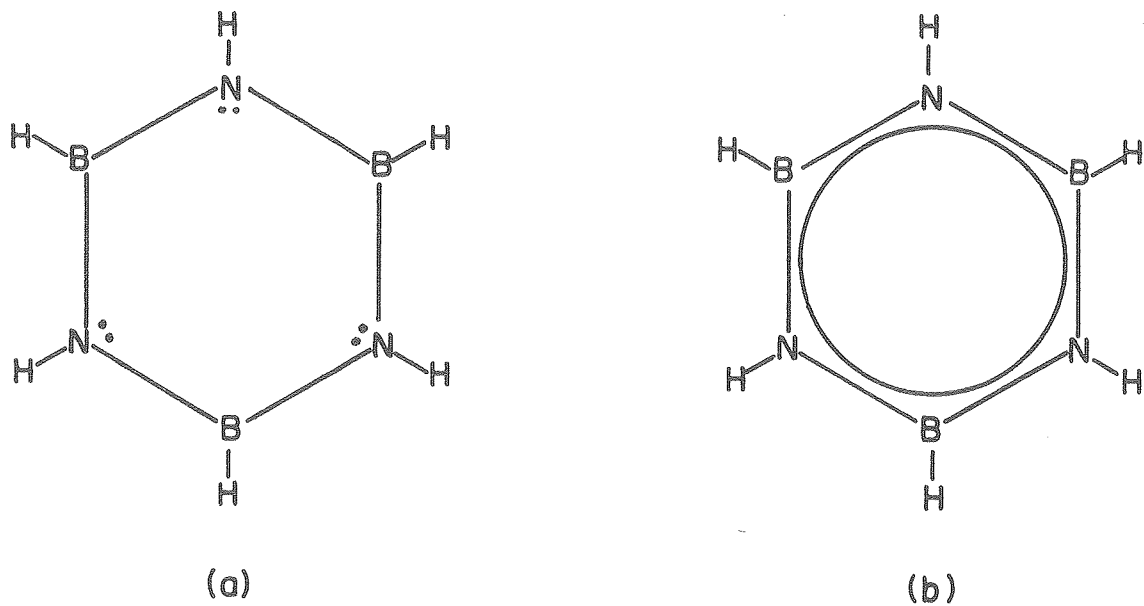
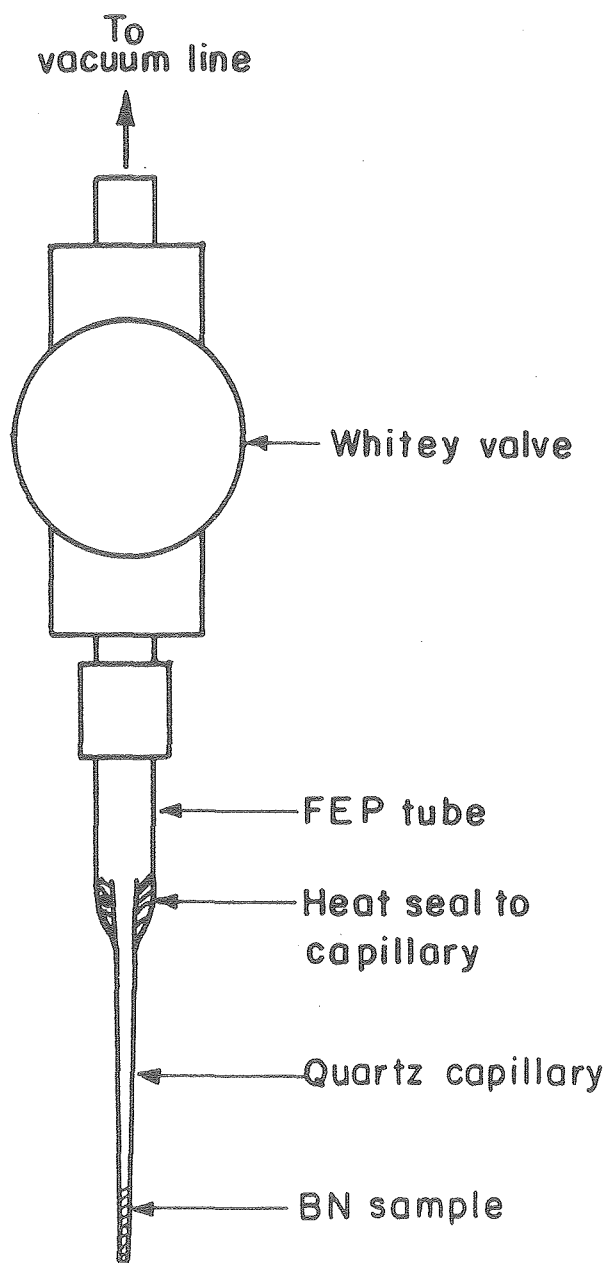Figure 5-1. Comparison of graphite and boron nitride structures.
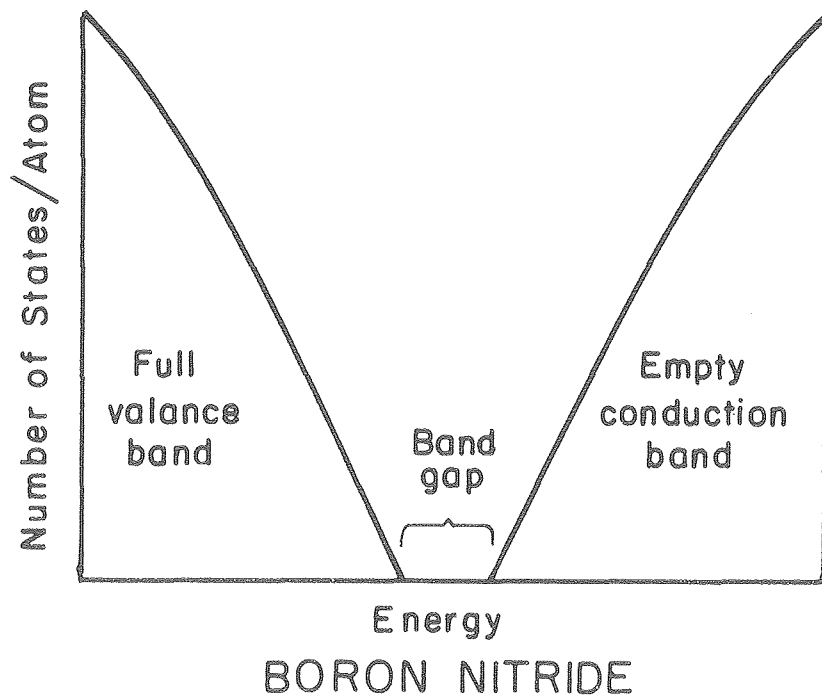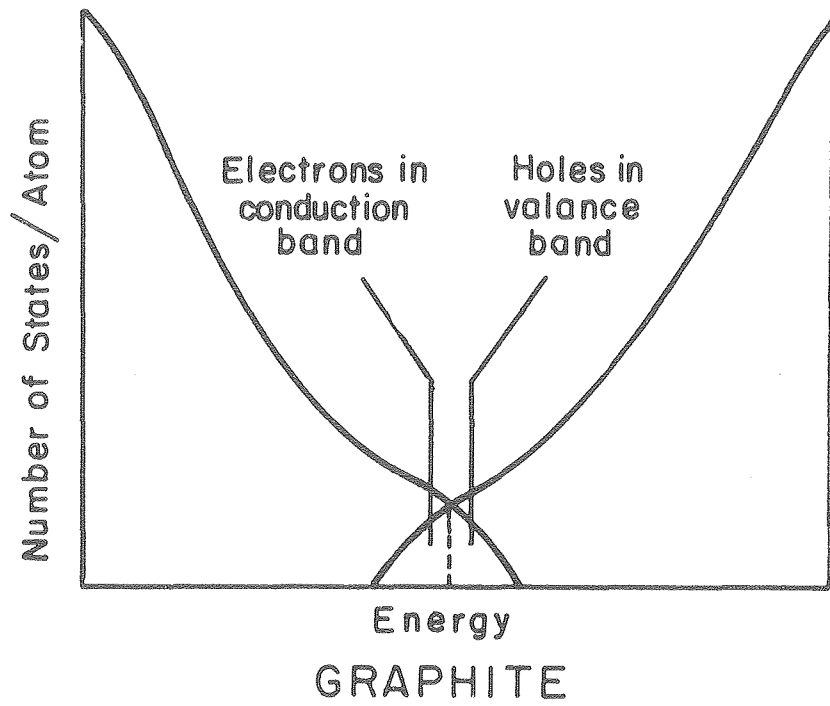
Figure 5-2. Graphite and boron nitride band structures.

(a)

(b)

XBL 8010-6003A

Figure 5-3. Bonding models for borazine, a) single bond, localized
and b) delocalized.

Figure 5-4. Reactor for reacting BN with $S_2O_6F_2$ in a capillary.

Appendix: Computer program for x-ray intensity data studies.

Program written in COMODORE BASIC for Comodore PET computer.

```
100 DIMA$(15),A1(15),B1(15),A2(15),B2(15),A3(15),B3(15),A4(15),B4(15),C(15)
101 DIM M(15),Z(15),B(15),A%(15)
102 DIM F0(20,5),F1(20,5),F2(20,5),FF(20)
105 M$="xxxxxxxxxxxxxxxxxxxxxxxxxxxxxxxxxxxxxxxxxxxxxxxxxxxxxxxxxxxxxxxxxxxxxxxxxx"
110 A$(1)="CARBON":A1(1)=2.31:B1(1)=20.8439:A2(1)=1.02:B2(1)=10.2075
111 A3(1)=1.5886:B3(1)=.5687:A4(1)=.865:B4(1)=51.6512:C(1)=.2156
112 A$(2)="OXYGEN":A1(2)=3.0485:B1(2)=13.2771:A2(2)=2.2868:B2(2)=5.7011
113 A3(2)=1.5463:B3(2)=.3239:A4(2)=.867:B4(2)=32.9089:C(2)=.2508
114 A$(3)="FLUORINE":A1(3)=3.5392:B1(3)=10.2825:A2(3)=2.6412:B2(3)=4.2944
115 A3(3)=1.517:B3(3)=.2615:A4(3)=1.0243:B4(3)=26.1476:C(3)=.2776
116 A$(4)="PHOSPHOROUS":A1(4)=6.4345:B1(4)=1.9067:A2(4)=4.1791:B2(4)=27.157
117 A3(4)=1.78:B3(4)=.526:A4(4)=1.4908:B4(4)=68.1645:C(4)=1.1149
118 A$(5)="SULFUR":A1(5)=6.9053:B1(5)=1.4679:A2(5)=5.2034:B2(5)=22.2151
119 A3(5)=1.4379:B3(5)=.2536:A4(5)=1.5863:B4(5)=56.1720:C(5)=.8669
120 A$(6)="GERMANIUM":A1(6)=16.0816:B1(6)=2.8509:A2(6)=6.3747:B2(6)=.2516
121 A3(6)=3.7068:B3(6)=11.4468:A4(6)=3.683:B4(6)=54.7625:C(6)=2.1313
122 A$(7)="ARSENIC":A1(7)=16.6723:B1(7)=2.6345:A2(7)=6.0701:B2(7)=.2647
123 A3(7)=3.4313:B3(7)=12.9479:A4(7)=4.2779:B4(7)=47.7972:C(7)=2.531
124 A$(8)="IRIDIUM":A1(8)=27.3049:B1(8)=1.59279:A2(8)=16.7296:B2(8)=8.86553
125 A3(8)=15.6115:B3(8)=.417916:A4(8)=5.83377:B4(8)=45.0011
126 A$(9)="O3F":A1(9)=3.1712:B1(9)=12.5285:A2(9)=2.3754:B2(9)=5.3494:C(8)=11.47
    2
127 A3(9)=1.539:B3(9)=.3083:A4(9)=.9063:B4(9)=31.2186:C(9)=.2575
190 INPUT "TITLE";AA$
200 INPUT "C-SPACING";C
205 INPUT"STAGE";R
210 INPUT "NUMBER OF UNIQUE ATOMS";NA
220 FOR I=1 TO 9:PRINT I,A$(I):NEXT
230 INPUT"ANY NEW ATOMS";T$
240 IF LEFT$(T$,1)="N" THEN 280
250 INPUT"WHAT ELEMENT";A$(I)
260 INPUT"A1,B1,A2,B2";A1(I),B1(I),A2(I),B2(I)
265 INPUT"A3,B3,A4,B4,C";A3(I),B3(I),A4(I),B4(I),C(I)
270 FOR M=1TOI:PRINT M,A$(M):NEXTM
275 I=I+1:GO TO 230
280 PRINT "ATOM#1 IS ALLOWED TO VARY,  FIRST INPUT PARAMETERS FOR FIXED ATOMS"
290 PRINT: PRINT "INPUT ATOM CODE,Z,MULTIPLICITY,THERMAL FACTOR"
300 FORI=2TONA:PRINT I;:INPUT A%(I),Z(I),M(I),B(I):NEXTI
310 PRINT "ASSIGN PARAMETERS FOR ATOM #1"
320 INPUT "ATOM TYPE";A%(1)
330 INPUT"VARY Z(0),MULTIPLICITY(1), OR THERMAL FACTOR(2)";V
331 IF V=1 THEN 360
332 IF V=2 THEN 380
335 INPUT"INITIAL,FINAL Z";ZI,ZF
340 INPUT"HOW MANY STEPS,1 TO 5";N:IFN=1 THEN 346
345 DZ=(ZF-ZI)/(N-1)
346 Y=ZI:YY=DZ
350 INPUT"MULTIPLICITY,THERMAL FACTOR";MI,BI
355 GO TO 410
```

```
360 INPUT"INITIAL,FINAL MULTIPLICITIES";MI,MF
362 INPUT"HOW MANY STEPS 1 TO 5";N:IF N=1 THEN 366
365 DM=(MF-MI)/(N-1)
366 Y=MI:YY=DM
370 INPUT"Z,THERMAL FACTOR";ZI,BI
375 GO TO 410
380 INPUT"INITIAL,FINAL THERMAL FACTOR";BI,BF
382 INPUT"HOW MANY STEPS 1 TO 5";N:IF N=1 THEN 390
385 DB=(BF-BI)/(N-1)
390 Y=BI:YY=DB
395 INPUT"Z,MULTIPLICITY";ZI,MI
410 OPEN1,4:OPEN2,4,1:OPEN3,4,2
420 FORI=1TO10
430 SL=I*1.5418/(2*C):TH=ATN(SL/SQR(-SL*SL+1)):S=I/(2*C):FP=0:SS=-S↑2
435 L1=(1+.82*COS(2*TH)↑2)/SIN(2*TH):L2=(1+COS(2*TH)↑2)/(SIN(2*TH)*SIN(TH))
440 FOR J=2TONA
450 Q=EXP(B(J)*SS)*M(J)*COS(2*π*I*Z(J))
460 X=A%(J):GOSUB 725:FP=FP+Q*SF
461 NEXTJ
470 FOR K=0TO(N-1)
480 Q=EXP((BI+DB*K)*SS)*(MI+K*DM)*COS(2*π*I*(ZI+K*DZ))
490 X=A%(1):GOSUB 725:F0(I,K)=FP+Q*SF
500 F1(I,K)=(F0(I,K)):F2(I,K)=(F0(I,K)↑2*L2)
510 NEXT K
520 FF(I)=10*FP:NEXT I
521 FOR J=0TO(N-1):R2(J)=F2(R+1,J)/1000
522 FORW=1TO10:R1(J)=R1(J)+ABS(F0(W,J))/1000:NEXTW
523 NEXT J
524 FORI=1TO10:FORJ=0TO(N-1):F1(I,J)=INT(F1(I,J)/R1(J)):F0(I,J)=INT(10*F0(I,J))
525 F2(I,J)=INT(F2(I,J)/R2(J)):NEXTJ:NEXTI
530 B$=" L      F(STAT)   ":C$="    Z( )    ":D$="                    "
531 Q$=CHR$(29):E$="    B( )    "
535 PRINT#1,CHR$(1);AA$:PRINT#1:PRINT#1,"C-SPACING = ";C;"   FOR STAGE ";R
540 PRINT#1:PRINT#1,"PARAMETERS FOR STATIONARY ATOMS"
550 PRINT#1,"   #  TYPE            Z       MULT     B"
560 PRINT#3," 99 AAAAAAAAAAAAAA 9.999     99.99     9.999"
570 FORI=NATO2STEP-1:PRINT#2,I;A$(A%(I));Q$;Z(I);M(I);B(I):NEXT I
575 PRINT#1
580 PRINT#1,"INITIAL PARAMETERS FOR ATOM #1"
590 PRINT#2,1;A$(A%(1));Q$;ZI;MI;BI
591 PRINT#1:PRINT#1:PRINT#1
600 IF V=2 THEN C$=E$
610 IF V=1 THEN C$="    M( )    "
620 FOR I=1TO N:B$=B$+C$:G(I)= Y+YY*(I-1)
630 D$=D$+STR$(I)+"        ":NEXT I
640 PRINT#1,B$;CHR$(141);:PRINT#1,D$
650 PRINT#3,"              AAAAA     AAAAA     AAAAA     AAAAA     AAAAA"
660 PRINT#2,STR$(G(1));Q$;STR$(G(2));Q$;STR$(G(3));Q$;STR$(G(4));Q$;STR$(G(5))
670 H$="  99    999999-   999999-   999999-   999999-   999999-   999999-    AAA
"
680 PRINT#3,H$
690 FORI=1TO10:PRINT#2,I;FF(I);F0(I,0);F0(I,1);F0(I,2);F0(I,3);F0(I,4);"F"
700 PRINT#2,0;0;F1(I,0);F1(I,1);F1(I,2);F1(I,3);F1(I,4);"F REL"
710 PRINT#2,0;0;F2(I,0);F2(I,1);F2(I,2);F2(I,3);F2(I,4);"I PC"
715 PRINT#1:PRINT#1,M$:PRINT#1
720 NEXT I
721 PRINT#1:PRINT#1,"PROGRAM 8/28/80 10:00 AM"
722 PRINT#1,CHR$(1);AA$
723 PRINT#1:PRINT#1:PRINT#1:PRINT#1:PRINT#1:PRINT#1:PRINT#1:PRINT#1:PRINT#1
724 STOP
725 YX=A3(X)*EXP(B3(X)*SS)+A4(X)*EXP(B4(X)*SS)+C(X)
726 SF= A1(X)*EXP(B1(X)*SS)+A2(X)*EXP(B2(X)*SS)+  YX
727 RETURN
730 END
```

ACKNOWLEDGMENTS

I would like to thank Professor Neil Bartlett for his help and guidance through the many trying times of my graduate career.

Special thanks goes to Mr. Howard Wood for his machine shop course, which proved invaluable. I would like to also thank my many coworkers in the lab, and the people in the support shops for their technical assistance and personal encouragement. Thanks also to Jim Boyer for all his work on the ill-fated heat capacity study, which never made it into this thesis.